

Arctic Landfast Sea Ice

by

Christof S. König

A dissertation submitted in partial fulfillment

of the requirements for the degree of

Doctor of Philosophy

Center for Atmosphere Ocean Science

Department of Mathematics

New York University

January 2007

David M. Holland – Adviser

To Marisa.

Acknowledgements

Firstly, I want to thank my adviser David Holland for guiding me through this time at Courant. His sense of humor and open-minded intellectual curiosity will hopefully remain with me for the times to come. He (and the tragic events of September 11, 2001) is also responsible for getting me onto icebreakers and igniting my affection for the Arctic.

To make my Arctic fieldwork possible, I also owe greatly to David Barber, Martin Fortier and Louis Fortier (no kinship) for taking me on board. There are too many fellow ship-goers to mention that made the time that I spent up there into one of the best times of my life but I would like to mention Lisa Miller, Peter Minnett, Tim Papakyriakou, Jody Deming, Anna Prokopowicz, Owen Owens, C. J. Mundy, Sonia Brugel, Katharine Cherewyk, Debbie Armstrong, and Romain Lanos.

Then I would like to express my gratitude to the CAOS and Courant faculty, which made even the time not spent on ships worth my while. Particularly

I thank Oliver Bühler, Shafer Smith and Olivier Pauluis for their sustained interest in the CAOS student activities.

This leads me to my fellow students at the institute: Without them this would truly have been a sad time in New York, particularly with Arjun Raj and Tyler Neylon I spent a lot of time studying as well as not studying. Further I would like to mention Helga Schaffrin Huntley, Andrea Barreiro, David Hammond, Ross Tulloch, Lyuba Chumakova, Fred Laliberté, Dan Goldberg, Minoru Kadota, as well as Miranda Holmes and thank them for the varying degrees with which they influenced my intellectual and extra-curricular life.

I also would like to thank the two undergraduate researchers that I worked with over two summers, Anna Mazover and Awad Ahmed. Besides enriching my summers, they asked many a “easy” question that stumped me and made me look it up. I also wanted to show my gratitude to all the undergraduate students that I have been teaching over the years at NYU. While the teaching was often competing with my research, it was also a place where the results of my labor were more immediately and readily visible; which can be crucial in those dark times.

I want to thank my parents and siblings very much for all their support. It has been a long time that I spent far away and I am very grateful that they have not given up on their “lost” son.

Finally, I reserve my greatest thanks for Marisa König Beatty who had to

endure quite some ups and downs during the whole process. May we go through many more of them together, it's so much more friendly with two (Piglet, 1926).

Abstract

Landfast ice is sea ice which forms and remains fixed along a coast, where it is attached either to the shore, or held between shoals or grounded icebergs.

Landfast ice fundamentally modifies the momentum exchange between atmosphere and ocean, as compared to pack ice. It thus affects the heat and freshwater exchange between air and ocean and impacts on the location of ocean upwelling and downwelling zones. Further, the landfast ice edge is essential for numerous Arctic mammals and Inupiat who depend on them for their subsistence.

The current generation of sea ice models is not capable of reproducing certain aspects of landfast ice formation, maintenance, and disintegration even when the spatial resolution would be sufficient to resolve such features.

In my work I develop a new ice model that permits the existence of landfast sea ice even in the presence of offshore winds, as is observed in nature. Based on viscous-plastic as well as elastic-viscous-plastic ice dynamics I add tensile

strength to the ice rheology and re-derive the equations as well as numerical methods to solve them. Through numerical experiments on simplified domains, the effects of those changes are demonstrated.

It is found that the modifications enable landfast ice modeling, as desired.

The elastic-viscous-plastic rheology leads to initial velocity fluctuations within the landfast ice that weaken the ice sheet and break it up much faster than theoretically predicted. Solving the viscous-plastic rheology using an implicit numerical method avoids those waves and comes much closer to theoretical predictions.

Improvements in landfast ice modeling can only be verified in comparison to observed data. I have extracted landfast sea ice data of several decades from several sources to create a landfast sea ice climatology that can be used for that purpose.

Statistical analysis of the data shows several factors that significantly influence landfast ice distribution: distance from the coastline, ocean depth, as well as the strength of offshore winds during nine out of the twelve months each year. Additionally, I identify regions where landfast ice appearance has been increasing or decreasing over the observed time span.

Contents

Dedication	iii
Acknowledgements	iv
Abstract	vii
List of Figures	xi
List of Tables	xvi
1 Introduction	1
1.1 The Arctic Ocean in the Global Climate	1
1.2 Landfast Sea Ice	3
1.3 Sea-Ice Physics	5
1.4 Current Sea Ice Models	15
2 Data on Landfast Sea Ice	18
2.1 Data Acquisition	18

2.2	Statistical Analysis	32
2.3	Results	33
2.4	Discussion	39
2.5	Data Acknowledgments	42
3	Modeling	43
3.1	Introduction	43
3.2	Momentum Equation	47
3.3	Modified Sea Ice Rheology	49
3.4	Conservation Laws	58
3.5	One-dimensional Numerical Implementation	60
3.6	Results	72
3.7	Discussion	85
	Bibliography	87

List of Figures

1.1	Landfast sea ice in the Beaufort Sea (Northwestern Canada). . .	4
1.2	The four possible stresses in two dimensions.	6
1.3	Some material under tensile strength.	8
1.4	A sample stress-strain diagram typical of structural steel. . . .	9
1.5	Stress-strain rate diagrams of materials with different plastic or viscous behavior. The dotted line shows an ideal Newtonian fluid.	11
1.6	Mohr's circle. The dashed lines hint on how the circle is con- structed from σ_{11} , σ_{12} and σ_{22} . The left and right most points of the circle are the principal stresses σ_1 and σ_2	13
1.7	Three different examples for yield curves (see text for explanations).	15
1.8	On large scales, sea ice is highly fragmented. This picture was taken from a height of approximately 1 km and shows an area of a few square kilometers.	16

1.9	Four different yield curves used in sea-ice models (from Zhang and Rothrock, 2005).	17
2.1	The egg code (from CIS, 2002)	23
2.2	Number of valid data from 1953 - 1998 at each location after the interpolation steps. Maximum number of data is 411. Land area is shown in brown.	29
2.3	Scatter plot (top) and contour lines of data density (bottom) of ocean depths versus their distance to coast. Contour lines are shown every $10^{0.25}$. Data density is measured in number of data per 0.2 degrees distance and per 200 m depth. The red line shows the linear correlation between the two.	31
2.4	Scatter plot (left) and contour lines of the logarithm of data density (right) of offshore wind strengths versus landfast sea-ice concentrations for all January data. Contour lines are shown every $10^{0.25}$. Data density is measured in number of data per m/s and per 2.5% of landfast sea ice concentration. The red lines show the linear correlation between the two.	34

2.5	<p>β coefficients of regressions of depth respective distance to coast versus landfast sea-ice concentration and their 95% confidence intervals. The upper curve shows the β coefficients with respect to ocean depth (in % landfast ice concentration per km), while the lower curve shows the β coefficients with respect to distance to coast (in % landfast ice concentration per degree solid angle).</p>	36
2.6	<p>β coefficients of regressions of offshore wind strength versus landfast sea-ice concentration and their 95% confidence intervals (blue). From April to June the β coefficients are not significantly different from zero (black line). The β coefficient and 95% confidence interval of the regression using all data is shown in red.</p>	37
2.7	<p>Significant changes of landfast sea-ice concentration over time. Red means a significant decrease and blue a significant increase in landfast ice concentration. Yellow signifies no significant change, while grey stands for missing data. Brown is land.</p>	38
2.8	<p>Percentage of landfast ice occurring at or below a certain depth. For example, 50% of landfast ice occurs at depths below 25 meters, or around 20% of landfast ice occurs on oceans deeper than 160 meters. This curve goes above a depth of zero because depths have been averaged over a 0.2 by 0.2° box.</p>	40

3.1	Relationship between the principal components of stress (σ_1 and σ_2) for a viscous-plastic rheology that allows for tensile strength.	50
3.2	Idealized schematic of a Maxwell material.	56
3.3	One-dimensional stress-strain rate diagram for a viscous-plastic material.	62
3.4	The staggered grid used in the one-dimensional model. u 's denote velocity points, while σ 's label material points, at which the equivalent ice thickness h and ice concentration a are also defined.	63
3.5	Stress (slanted line) in an idealized piece of landfast ice (dashed) under the influence of a constant offshore wind.	73
3.6	Profiles of equivalent ice thickness h as modeled by the implicit implementation of the viscous-plastic rheology. On the left side are the results of the regular model without tensile strength initially, after 2.5 days and after 3.5 days. On the right side are the results after adding tensile strength at the same times.	76
3.7	Ice velocities within the 100 km of landfast ice after one time step (10 min's) using the implicit solver. In this graph, the analytical solution would be indistinguishable from this curve.	77

3.8	Profiles of equivalent ice thickness h . The figures to the left show the solution as found using the implicit scheme, the right side the results using EVP. The top shows the initial condition, the middle two pictures show the state after 2.5 days, the bottom after 3.5 days.	78
3.9	The top two figures show the equivalent ice thickness after 0.5, 2.5 and 3.5 days (top to bottom). The figures to the left show the solution as found using the implicit scheme, the right side the results using EVP. Only the first 100 km are shown (ice extent). Note that the scales differ between the left and the right column.	80
3.10	Initial velocity fluctuations (on top) and the development of the ice thickness during the same time (on the bottom).	81
3.11	Initial velocity fluctuations in the EVP model. The top figure shows velocities when using a time step of 10 minutes, while the bottom figure uses a time step of 1 minute. Note the different scales in time as well as velocities.	83
3.12	Number of days until landfast ice of a certain width breaks off under the influence of offshore wind.	84

List of Tables

2.1	Codes that can appear in DEX files instead of egg codes.	25
2.2	Correlations between topographical parameters and landfast sea- ice concentration.	35
3.1	Constants and parameters used in the landfast sea ice model. . .	51
3.2	Default setup of the one-dimensional model.	71

Chapter 1

Introduction

1.1 The Arctic Ocean in the Global Climate

Our climate is warming as the sustained combustion of fossil fuel increases the atmospheric concentrations of greenhouse gases that trap solar energy. Despite the Kyoto Protocol, there is no indication that the rate of increase of atmospheric concentrations of greenhouse gases will be significantly curbed in the foreseeable future. According to numerical models of future climate, warming of the atmosphere will start and be most intense in the Arctic (e.g. Stouffer et al. (1989), Shindell et al. (1999)). By 2070, the lower atmosphere north of the Arctic Circle is predicted to warm by 2.2 to 3.9°C (ACI, 2001).

Consistent with this prediction, the extent of Arctic sea-ice has been decreasing by 0.35% per year since the 1970's for a total reduction of about 14%

(Johannessen et al., 1995). Of even bigger concern is that the thickness of the multi-year ice pack that covers the central Arctic Ocean has diminished by 40% in the 30 years from the 1960's to the 1990's (Rothrock et al., 1999).

Within the Arctic Ocean, changes in ice extent, thickness and season in response to global warming are expected to occur first and be most pronounced on the shallow peripheral shelves (Macdonald et al., 1995). The Arctic shelves form 25% of the global shelf area and cover roughly a third of the Arctic Ocean basin.

While atmospheric forcings like wind and temperature are the most important factors influencing sea ice formation in the Arctic Ocean (Tremblay and Mysak, 1998), on the shelves, freshwater discharge from rivers also plays a significant role. 10% of global river discharge empties into the Arctic basin and not only bring an immense amount of freshwater (2000 km³ per year) but also carbon and other nutrients.

The sea ice cover determines the air-sea exchange of heat and moisture over the Arctic Ocean and constrains the small window of biological productivity of the Arctic marine ecosystem (Rysgaard et al., 1999). By increasing photosynthetic fixation of atmospheric carbon through a reduction of ice cover, climate warming may profoundly alter biogeochemical fluxes on Arctic shelves, there-

fore affecting the export of carbon to the pelagic¹ and benthic² food webs, and to the deep basins where it can be sequestered.

Whatever the causes of the observed reduction of Arctic sea ice (anthropogenic or cyclic), the assessment of its potential impacts requires a significant improvement of our understanding of the processes and feedbacks linking freshwater, sea ice, climate, biological productivity and biogeochemical cycles in the Arctic in general and on Arctic shelves in particular.

1.2 Landfast Sea Ice

Landfast ice is sea ice that forms and remains fixed along a coast, where it is either attached to the shore or held between shoals or grounded icebergs. It covers Arctic shelves during large portions of the year, normally starting to form in October and reaching its widest extent during April and May (Barber and Hanesiak, 2004, Divine et al., 2005, Volkov et al., 2002).

Due to its lack of mobility, landfast ice fundamentally modifies the momentum exchange between atmosphere and ocean. It covers the shelf area for four to eight months each year and thus greatly affects the heat and freshwater exchange there. The freezing and melting of landfast ice make important contributions to salt and freshwater budgets, thereby influencing water circulation,

¹Pelagic: in the open water, away from the sea bottom

²Benthic: relating to the bottom of a body of water.

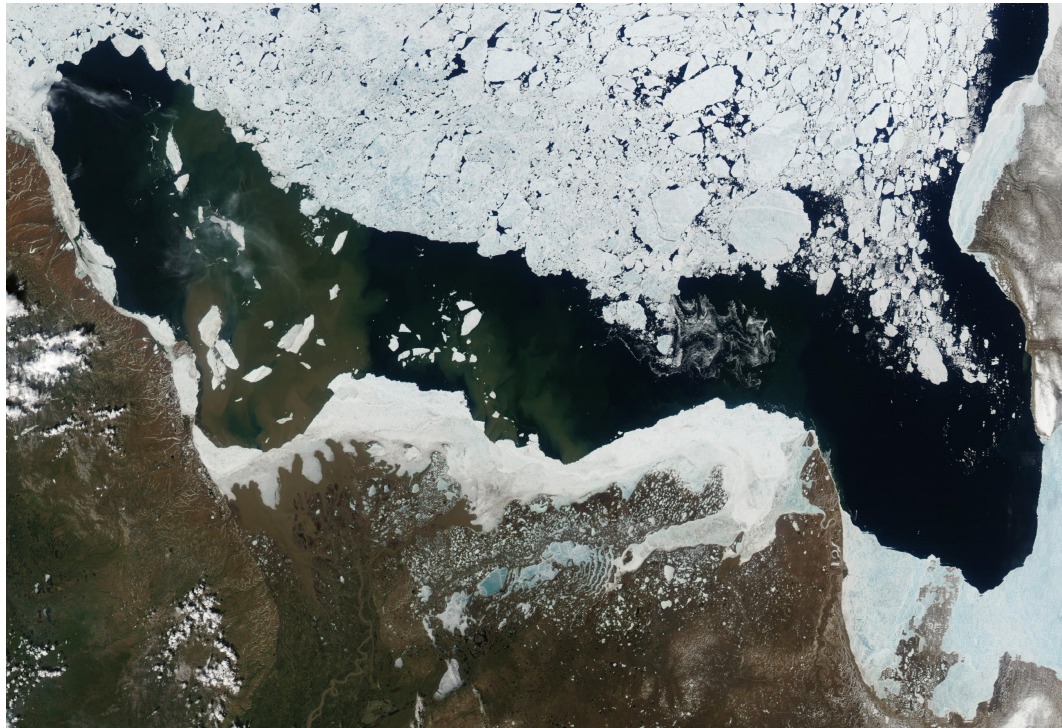


Figure 1.1: Landfast sea ice in the Beaufort Sea (Northwestern Canada).

dense water production and the location of upwelling and downwelling zones (Macdonald et al. (1999)).

Besides being a strong influence on the whole coastal oceanic ecosystem, the landfast ice edge is also essential for numerous Arctic mammals and Inupiat who depend on them for their subsistence (Tynan and DeMaster, 1997).

1.3 Sea-Ice Physics

To model sea-ice dynamics we have to know or approximate the forces that act on the ice. Most of those forces require us to know winds, as well as ocean currents and sea surface tilt (Coon, 1980, Rothrock, 1975). Atmospheric forcing seems to be the most dominant influence on sea ice movement (Coon, 1980) and also particularly on fast ice break up (Divine et al., 2005).

Early models thus used free drift formulations ignoring ice interactions or concentrated on thermodynamical effects (Bryan et al., 1975, Felzenbaum, 1961, Manabe et al., 1979).

However the interaction of sea ice with itself is an important effect (Coon, 1980, Hibler, 1979, 1986, Parkinson and Washington, 1979), which shall be described in this section. The study of deformation and flow of sea ice is called *sea-ice rheology*. The same expression is often also used to denote a particular model for sea ice (e.g. viscous-plastic sea-ice rheology).

Sea ice is generally modeled as a two-dimensional non-Newtonian fluid between atmosphere and ocean (e.g. Pritchard, 1975) as tracking individual ice floes is intractable. To reduce the three dimensions to two, one has to integrate ice properties like ice stress over its thickness. The force due to the variation in vertically integrated internal ice stress appears in the momentum equations

(3.1) as

$$\frac{\partial \sigma_{ij}}{\partial x_j} \tag{1.1}$$

where σ_{ij} is the stress in j -direction acting on a plane which is perpendicular to the i -axis (see Figure 1.2). Repeated indices (in this case j) are being summed over, in this case to get the sum of all forces acting in i -direction. If i and j are identical we speak of “normal stress” if they differ we speak of “shear stress”. Shear stresses often are also called τ_{ij} . i and j can be set to x and y or 1 and 2 with identical meaning. Here I use the latter.

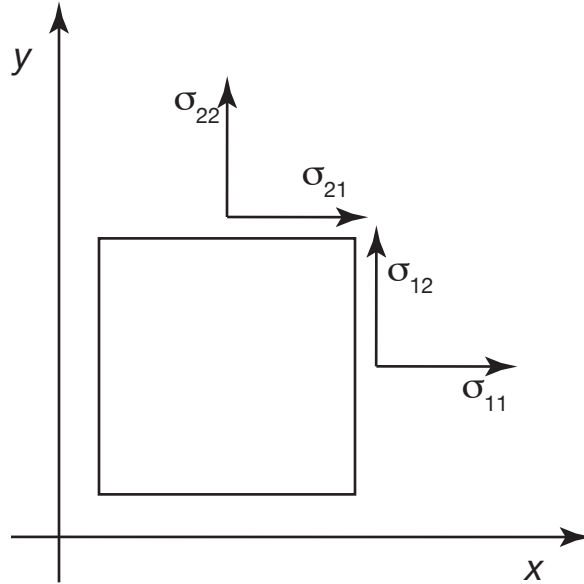


Figure 1.2: The four possible stresses in two dimensions.

We vertically integrated the stresses over the ice thickness because we ignore possible variations. Firstly, sea ice is very thin (on the order of meters) as com-

pared to its extent (order of tens to hundreds of kilometers), so that variations over its thickness seem negligible. Secondly, very little is known about stress variations inside sea ice.

Stress normally has the same units as pressure, $\frac{\text{N}}{\text{m}^2}$. The material variables we use are all relative to unit area though, and additionally we integrated the stresses over the ice thickness, so that the stresses used here end up having units of $\frac{\text{N}}{\text{m}}$, respectively $\text{Pa} \cdot \text{m}$ or $\frac{\text{kg}}{\text{s}^2}$ (Rothrock, 1975).

In our two-dimensional case, the stress tensor contains four elements as shown in Figure 1.2. Except for cases where a rotational force is applied to the inside of the fluid (for example via suspended ferromagnetic particles in a magnetic field) the stress tensor is symmetric, i.e. $\sigma_{12} = \sigma_{21}$ (Acheson, 1990) meaning that we have three stress variables.

To find the ice stresses, we have to relate them to other properties of the ice field, like ice velocities, thickness or concentration. To do this we look for inspiration in the material sciences.

1.3.1 Mechanics of Solid Materials

Consider a specimen of a given material subjected to a tensile force P (see Figure 1.3). As the force increases we observe an absolute elongation Δ which is proportional to the length of the material L . The elongation per unit length

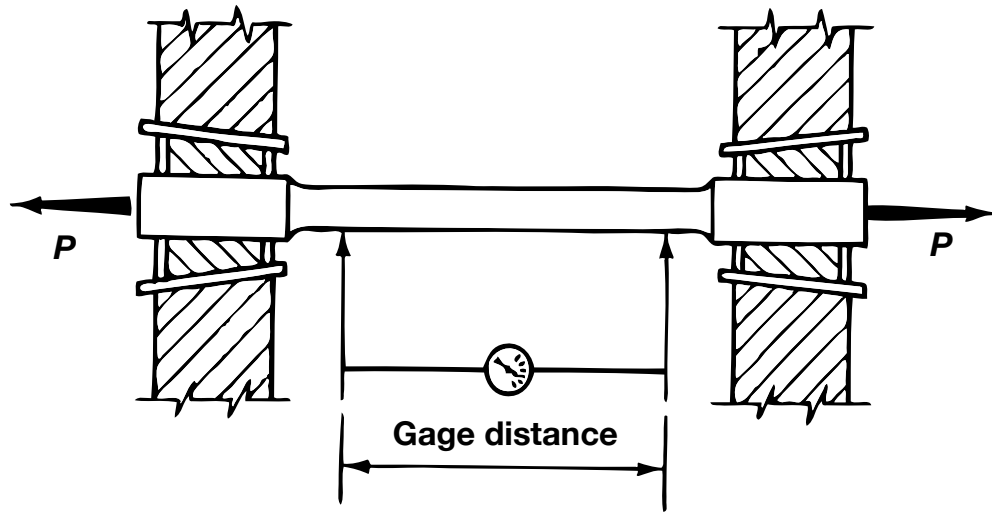


Figure 1.3: Some material under tensile strength.

ϵ is then

$$\epsilon = \frac{\Delta}{L} \quad (1.2)$$

ϵ is better known as *strain*.

The axial stress σ is the ratio of force per cross-sectional area

$$\sigma = \frac{P}{A} \quad (1.3)$$

and thus has the same units as pressure.

Elastic regime

Most materials behave elastically up to some point (point A in Figure 1.4), meaning the relationship between stress and strain is linear. This deformation is reversible, i.e. when the stress is removed, the strain will also go back to zero.

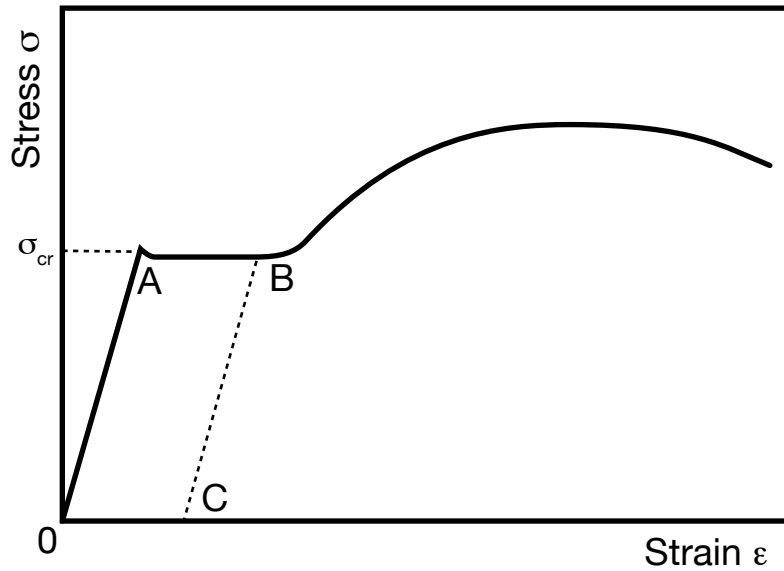


Figure 1.4: A sample stress-strain diagram typical of structural steel.

The slope of the line is called *modulus of elasticity* E . This relationship is also called *Hooke's law*:

$$E = \frac{\sigma}{\epsilon} \quad (1.4)$$

A similar relationship also exists for shear stresses, where while in the elastic regime the shear stress is proportional to the shearing strain with a proportionality constant called *shear modulus of elasticity*.

Plastic regime

Once the yield stress has been reached the relationship between strain and stress becomes non-linear. In Figure 1.4 we see that once point A is reached that without any increase in stress the strain will continue to increase up to a

point B. This is called the *plastic regime*. This deformation is irreversible, so if at point B the stress is decreased to zero, strain would not go back to the origin but down to C as the atomic structure had been destroyed locally.

The critical stress σ_{cr} where the elastic turns into plastic regime is called *yield stress*.

After point B other effects can happen. In the material shown in Figure 1.4 (steel) the stress again has to increase up to some maximum strength (strain hardening). Beyond, a neck forms where the local cross-sectional area decreases more quickly than the rest of the sample until it fractures. Other materials can have very different behavior from the one discussed here, particularly beyond point B.

We saw that once the critical stress σ_{cr} has been reached the strain can just keep on decreasing. In that regime we become interested in how quickly the strain will increase, i.e. we are more interested in how fast the strain changes over time, i.e. in the *strain rate* $\dot{\epsilon} = \frac{\partial \epsilon}{\partial t}$.

Viscosity

In an ideal plastic material the stress is independent of strain rate, which in a stress-strain rate diagram is shown as an horizontal line (see Figure 1.5). A slope in that curve is called *viscosity* μ .

A material without yield stress σ_{cr} that shows viscous behavior with a con-

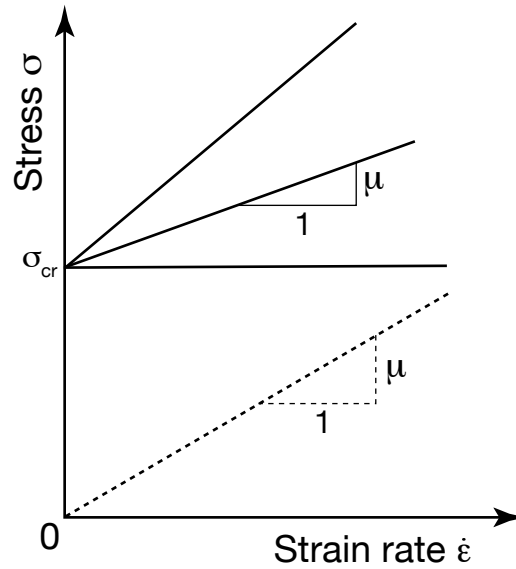


Figure 1.5: Stress-strain rate diagrams of materials with different plastic or viscous behavior. The dotted line shows an ideal Newtonian fluid.

stant slope μ as soon as a stress is applied is called a Newtonian fluid. Some early sea ice models (Campbell, 1965) treated the ice as Newtonian fluid.

1.3.2 Mohr's circle

As mentioned previously, in two dimensions the stress state is defined by the three variables σ_{11} , σ_{12} and σ_{22} . The specific values depend on the coordinate system chosen. When rotating the coordinate system those stress values would change.

To find more fundamental measures for stress we look at how those stresses change under rotation of the coordinate system. After rotating by an angle θ

normal and shear stresses become (see for example Popov, 1952)):

$$\sigma'_{11} = \frac{\sigma_{11} + \sigma_{22}}{2} + \frac{\sigma_{11} - \sigma_{22}}{2} \cos 2\theta + \sigma_{12} \sin 2\theta \quad (1.5)$$

$$\sigma'_{12} = \frac{\sigma_{11} - \sigma_{22}}{2} \sin 2\theta + \sigma_{12} \cos 2\theta \quad (1.6)$$

Interestingly, there is always an angle θ so that σ'_{12} becomes zero. This means that there is always a coordinate system that is oriented so that no shear stresses are experienced. At this same angle the normal stresses achieve their extremal values σ_1 respectively σ_2 :

$$\sigma_{1,2} = \frac{\sigma_{11} + \sigma_{22}}{2} \pm \sqrt{\left(\frac{\sigma_{11} - \sigma_{22}}{2}\right)^2 + \sigma_{12}^2} \quad (1.7)$$

σ_1 and σ_2 are called *principal stresses* and are the eigenvalues of the stress tensor.

Equations (1.5) and (1.6) can be manipulated to get the following relation:

$$\left(\sigma'_{11} - \frac{\sigma_{11} + \sigma_{22}}{2}\right)^2 + \sigma_{12}'^2 = \left(\frac{\sigma_{11} - \sigma_{22}}{2}\right)^2 + \sigma_{12}^2 \quad (1.8)$$

This equation describes a circle with center at

$$C = \left(\frac{\sigma_{11} + \sigma_{22}}{2}, 0\right)$$

and radius

$$r = \sqrt{\left(\frac{\sigma_{11} - \sigma_{22}}{2}\right)^2 + \sigma_{12}^2}$$

This circle is called *Mohr's circle* and shown in Figure 1.6. All points on this circle describe the same stress state in some material. If the coordinate system

is being rotated by an angle θ the stress state moves an angle of 2θ on the circle.

The coordinate of the center of the circle and the radius of the circle are called

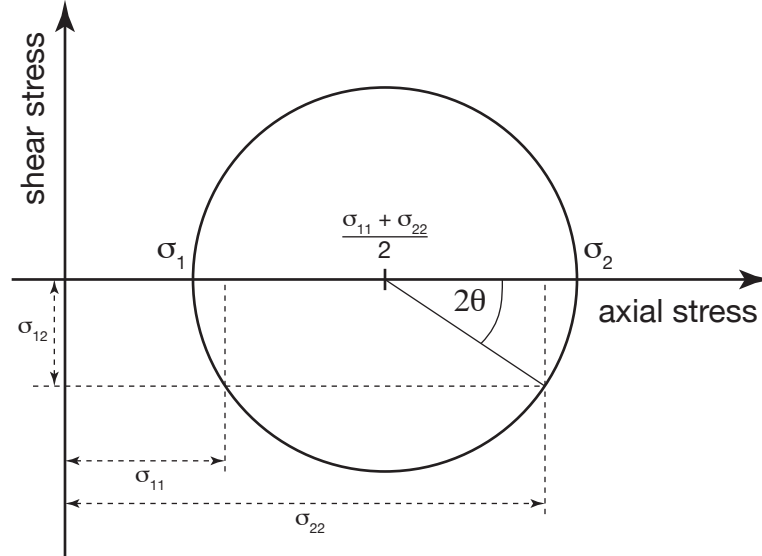


Figure 1.6: Mohr's circle. The dashed lines hint on how the circle is constructed from σ_{11} , σ_{12} and σ_{22} . The left and right most points of the circle are the principal stresses σ_1 and σ_2 .

the *stress invariants* σ_I and σ_{II} :

$$\sigma_I = \frac{\sigma_{11} + \sigma_{22}}{2} \quad (1.9)$$

$$\sigma_{II} = \sqrt{\left(\frac{\sigma_{11} - \sigma_{22}}{2}\right)^2 + \sigma_{12}^2} \quad (1.10)$$

Thus we end up with three different ways of defining stress states, two normal and one shear stress σ_{11} , σ_{22} , and σ_{12} ; the minimum and maximum (principal) normal stresses σ_1 and σ_2 ; or the two stress invariants σ_I and σ_{II} .

1.3.3 Yield criteria

We saw that materials that are being pulled apart have a critical yield stress σ_{cr} at which elastic behavior becomes plastic. A similar yield stress can be found by compressing the material. To differentiate among the two let's speak of the former as σ_{cr_T} (critical stress under tension), and of the latter as σ_{cr_C} (compression). In two dimensions, instead of two yield points we have a *yield curve*. Within the yield curve the material behaves like an elastic or viscous material, once the curve is reached, plastic deformation takes place. Some examples for such yield curves are given in Figures 1.7 and 1.9.

One simple assumption might be that a material has a maximum compressive (σ_{cr_C}) as well as tensile strength (σ_{cr_T}), ignoring that failure could happen due to shear stresses. The yield curve then becomes a square as shown in Figure 1.7 (solid line).

We should additionally consider that failure could also happen due to shear stresses. Mohr-Coulomb theory proposes that the critical shear strength should be proportional to the maximum normal stress, somewhat analogous to frictional forces. Adding this constraint we get the dashed yield curve, which is split into two parts by the origin.

If we assume that there is no shear strength whatsoever, the yield curve collapses onto the dash-dotted diagonal line.

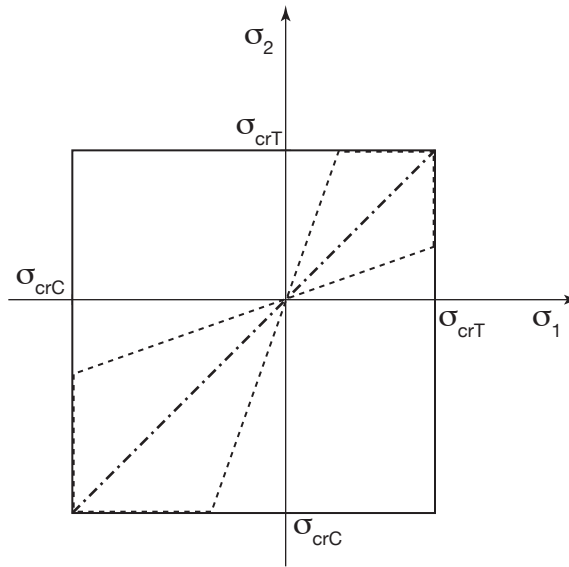


Figure 1.7: Three different examples for yield curves (see text for explanations).

1.4 Current Sea Ice Models

Sea ice models generally assume that sea ice does not have any tensile strength. This is justified on large scales as sea ice is generally broken up into pieces much smaller than grid-scales used in sea ice models (see Figure 1.8). That means that sea ice drifts apart without resistance when subjected to a divergent force. This implies a critical tensile yield strength of zero, meaning that yield curves are restricted to the third quadrant.

No tensile strength together with no shear strength (dash-dotted diagonal line in Figure 1.7 restricted to bottom-left quadrant) is for example being made by Flato and Hibler (1992) who call it cavitating fluid. Tremblay and Mysak (1997) reached a very similar rheology by assuming that ice is a granular mate-



Figure 1.8: On large scales, sea ice is highly fragmented. This picture was taken from a height of approximately 1 km and shows an area of a few square kilometers.

rial.

Mohr-Coulomb-type and square rheologies (see again Figure 1.7) have been used and compared by Ip et al. (1991).

Some other yield curves suggested for sea ice models are shown in Figure 1.9 (taken from Zhang and Rothrock, 2005, who compared them). The most prominent of those is the elliptical yield curve (Hibler, 1979, shown as a solid line) that has become the standard ice dynamics model according to Hunke and

Dukowicz (1997) even though it does not strictly remain in the third quadrant.

Coon et al. (1974) as well as Rothrock (1975) proposed teardrop-shaped yield curves. “MCE” stands for “Mohr-Coulomb-ellipse” and was proposed by Hibler and Schulson (2000) and is a combination of an elliptical yield curve with Mohr-Coulomb shear failure. The lens yield curve had been presented by Bratchie (1984).

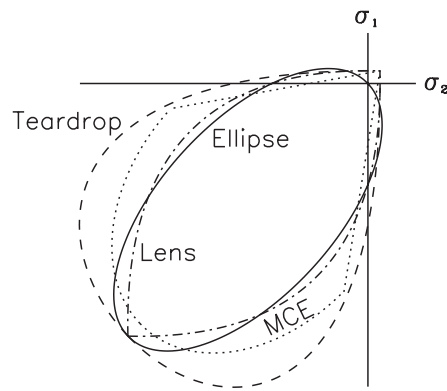


Figure 1.9: Four different yield curves used in sea-ice models (from Zhang and Rothrock, 2005).

Those models normally are being used without any tensile strength, but some studies (e.g. Zhang and Rothrock, 2005) use small tensile strengths with some rheologies as shown in Figure 1.9 to insure that energy is always being dissipated even under divergent creep (Schulkes, 1996), i.e. not on physical grounds but for reasons of numerical stability.

Chapter 2

Data on Landfast Sea Ice

In this chapter, I gather and analyze data on landfast sea ice to identify factors affecting landfast ice.

2.1 Data Acquisition

2.1.1 Russian Arctic and Antarctic Research Institute (AARI)

The National Snow and Ice Data Center¹ (NSIDC) offers a wide range of cryospheric data sets. The only extensive data set that contains landfast ice information is based on the Russian Arctic and Antarctic Research Institute's

¹<http://nsidc.org/>

(AARI) digital sea ice charts (Fetterer and Troisi, 1997a). AARI digitized Arctic sea ice concentration and stage of development (i.e. age and shape of ice) information from original paper source charts as part of an international data exchange program. The AARI source charts were developed from aircraft and satellite observations for shipping purposes, and provide extremely detailed information (Fetterer and Troisi, 1997b).

NSIDC provides AARI data in NSIDC's Equal Area SSM/I Earth (EASE) Grid. AARI sea ice data in the EASE-Grid North azimuthal projection are gridded at a 12.5 km resolution, for both Western (24W to 110E) and Eastern (105E to 130W) sectors. The area covered by the data varies greatly over time though.

Data extend from 1953 through 1990 (Fetterer and Troisi, 1997b). Normally, information is provided every 10 days, on the 5th, 15th and 25th of each month. In some years, data is much sparser though, particularly during the early years.

The AARI database provides five different types of sea ice data at each grid point in so-called "layers" as follows:

For this study, only the data from the fifth layer ("Fast ice area") was used. At any location, a 0 indicates that there was no landfast ice at that time while a 1 indicates its presence. In contrast to the Canadian data (see below) no partial coverage by landfast ice is being considered.

This data was extracted as a percentage (either 0 or 100), paired up with

1. Total sea ice concentration
2. Multi-year sea ice concentration
3. First-year sea ice concentration
4. New (or "younger") sea ice concentration
5. Fast ice area

its date and EASE grid longitude and latitude and written out to text files. A text format was chosen to guarantee maximal flexibility when merging this data with data from other sources.

Definition of landfast sea ice

AARI does not give a proper definition of landfast ice. The data stems from a variety of sources (aircraft observations, satellites, etc.) and was compiled by AARI employees, which presumably "know it when they see it".

2.1.2 Canadian Ice Service (CIS)

Definition of landfast sea ice

The Canadian Ice Service (CIS) defines *fast ice* as follows (CIS, 2002):

Ice which forms and remains fast along the coast. It may be attached to the shore, to an ice wall, to an ice front, between shoals

or grounded icebergs. Vertical fluctuations may be observed during changes of sea level. It may be formed "in-site" from water or by freezing of floating ice of any age to shore and can extend a few meters or several hundred kilometers from the coast. It may be more than one year old in which case it may be prefixed with the appropriate age category (old, second-year or multi-year). If higher than 2 m above sea level, it is called an ice shelf.

Data coverage and resolution

The Canadian Ice Service offers an extensive archive of ice charts on their web page². "Daily analysis Ice Charts" are available from 1999 onwards, while "Regional Ice Charts" can be obtained for 1968 - 2006. Over the winter months (December - May) they are provided at monthly intervals while they come at weekly intervals over the remaining summer months.

The data is provided for four different regions; for this study only data from the Western and Eastern Arctic were considered, which together reach approximately from 180°W to 40°W at a spatial resolution of approximately 10 km.

²<http://ice-glaces.ec.gc.ca/app/WsvPageDsp.cfm?ID=11700>

The Egg Code

CIS uses the so called “egg code” to describe ice conditions. The basic data concerning concentrations, stages of development (age) and form (floe size) of ice are contained in a simple oval form. A maximum of three ice types is described within the oval. This oval and the coding associated with it, are referred to as the “Egg Code” (CIS, 2002). This code conforms to international conventions by the World Meteorological Organization³.

Figure 2.1 is a summary diagram of the Egg Code.

The total concentration C_t refers to the total percentage of surface area that is covered by sea ice and is the sum of C_a , C_b and C_c (and possibly C_d), the partial area concentrations of different ice types in decreasing thickness and age (which in general is synonymous). If only one ice type is observed, C_t can be specified alone and the second row left empty. Concentration is specified in and rounded to tenths.

The next row refers to the stage of development, i.e. its age ranging from new and young ice to first-year ice types to multi-year ice. Each stage is coded by a one digit number with an optional dot to its right or a special sign. Numbers outside the oval refer to traces or to special occasions that appear rarely enough that they shall be ignored here. All the details about the interpretation of egg

³<http://www.wmo.ch/>

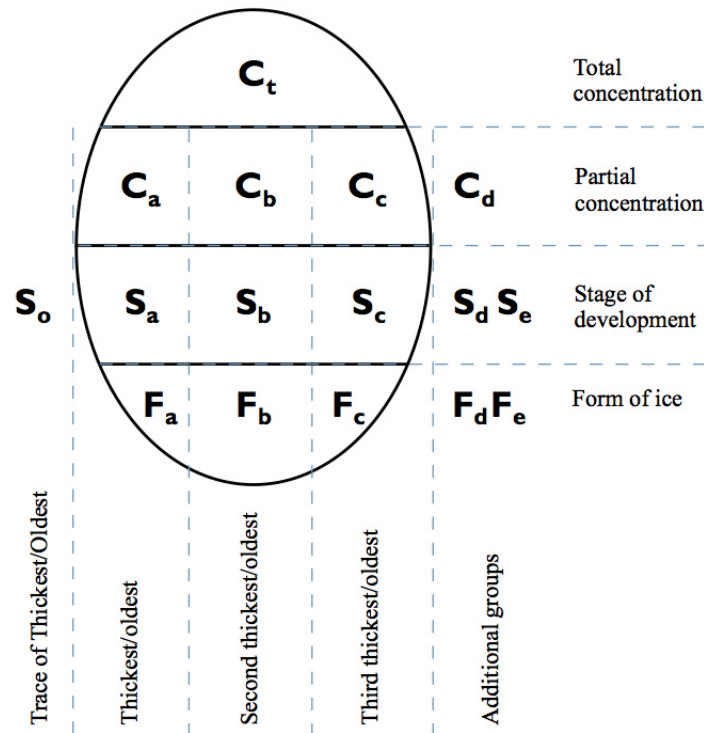


Figure 2.1: The egg code (from CIS, 2002)

codes can be found in CIS, 2002, which is freely downloadable.

The bottom row specifies the form of ice, going from pancake ice, brash, to all possible sizes of ice floes. Fast ice and icebergs are also specified here. Again different forms are represented by one digit numbers here, fast ice is represented by an “8”.

The values on different rows belong to each other, i.e. ice that is present with a concentration C_i is in a stage of development of S_i and of the form F_i . Thus to extract landfast sea ice information, one has to search the ”Form of

Ice” row (F_i) for “8” and then use the corresponding concentration above.

It should also be mentioned that - unlike the AARI data, which only gives 0 or 100% landfast ice - the Canadian data also provides landfast ice concentrations in between at 10% intervals.

CIS Data Formats

The data can be downloaded from CIS’s web page⁴ as GIF images or in an “e00” format that can be read by Geographic Information System (GIS) software. Upon request so-called dex files can be made available. Dex files are text files that contain 34 header lines, sea-ice data, and two final text lines. All the data contained in one file stems from one day. Due to those final two lines of text, loading the data was only found possible using FORTRAN routines.

A few typical data lines out of the data part of a dex file could look as follows:

```
81.75000    63.00000 10      7. 8
80.73762   101.08240 8      4  7. 6  4  6  6
80.00000    86.50000 0W
81.25000    69.00000 POINT NOT COVERED BY POLYGON
74.97086    80.14297 FAST
```

⁴<http://ice-glaces.ec.gc.ca/app/WsvPageDsp.cfm?ID=11700>

The first number on a line is the latitude, the second number is the negative longitude (i.e. longitude is increasing to the West) of the data point. This is followed by the “Egg Code” (see above) or one of the codes in table 2.1.

Table 2.1: Codes that can appear in DEX files instead of egg codes.

OW	Open Water
BW	Bergy Water
IF	Ice Free
FAST	Fast Ice
LAND	Land
POINT NOT COVERED BY POLYGON	No data available

The egg code in the dex files consists of a row of numbers as follows

Ct Ca Sa Fa Cb Sb Fb Cc Sc Fc So Sd

where the letter combinations correspond to the ones in figure 2.1.

Analyzing the dex files

Again, as with the data from AARI, any landfast ice information contained in the data was written out as text files with one datum on each line, starting with year, month and day, followed by latitude, longitude (up to an accuracy of a hundredth of a degree) and the landfast sea ice concentration in percent.

Firstly, the file name was used to find the time information.

Within the file, after the header lines were ignored, each line was read as two floating numbers (latitude and longitude) and a long “egg code string”. This string then first was checked if it began with **FAST**, in which case 100% landfast ice was assumed at that location.

Afterwards, if the first character of the egg code string was a number, the positions for **Fa**, **Fb** and **Fc** were checked for 8’s. If a 8 was found, the corresponding ice concentrations were used to find the local percentage of area covered by landfast sea ice. If no 8 was found, a concentration of zero was written out.

Lastly, if the egg code string was “**OW**”, “**BW**” or “**IF**” the landfast ice concentration was taken to be zero.

2.1.3 Landfast Ice Data Processing

After the landfast ice data was extracted from the two different sources and written out to text files, it was brought together and interpolated onto a common time and space grid. The interpolation was done in two steps, first a spatial gridding onto a regular longitude-latitude grid, then a time interpolation to find monthly means at each location.

Spatial Gridding

All the data from the same day was gridded onto a longitude-latitude grid with 0.2° resolution spanning latitudes from 55°N to 90°N and all longitudes. To this end, the following rules were applied:

- Only data within a great circle distance of 0.1° respectively 0.2° were considered.
- Only the three closest data points (or fewer) were used.
- Data was weighted with its inverse great circle distance to the interpolation point.

Wherever there was no data available that was close enough, "Not a Number" (NaN) was used to represent missing data.

Temporal Gridding

At each location, data was linearly interpolated over time. To average, the area under that curve was computed for a given month and divided by its length. If there was no data, for up to 30 days, constant landfast ice concentration was assumed. If there was no data for more than 30 days before or after, the monthly average was set to missing.

A linear development of the landfast ice concentration might not be very realistic, but any other interpolation scheme makes even more specific assumptions regarding the smoothness of fast ice behavior.

The total number of landfast ice data from 1953 - 1998 at each location can be seen in Figure 2.2. In particular note the sharp edge in the Western Canadian Arctic that will have an effect on the data analysis later. Also note that there is very little data to none along the Northern and Eastern coast of Greenland and along the Scandinavian coast.

The data is made available for download in Network Common Data Form (NetCDF) on the World Wide Web⁵.

2.1.4 Ocean Depth and Distance to Coastline

The topographical data used in this study was obtained from the International Bathymetric Chart of the Arctic Ocean⁶ (IBCAO). The IBCAO grid is a product of contour, grid, point, and track data. Depth data is provided at minute intervals between 64°N and 90°N and all longitudes. For this study, we used the 2-D NetCDF version provided by Ned Cokelet from NOAA/PMEL.

Depth data was obtained by averaging depth over a 0.2° square around each

⁵Select “Landfast Sea Ice” on <http://maud.cims.nyu.edu:8080/las/servlets/dataset?catitem=266>

⁶<http://www.ngdc.noaa.gov/mgg/bathymetry/arctic/>

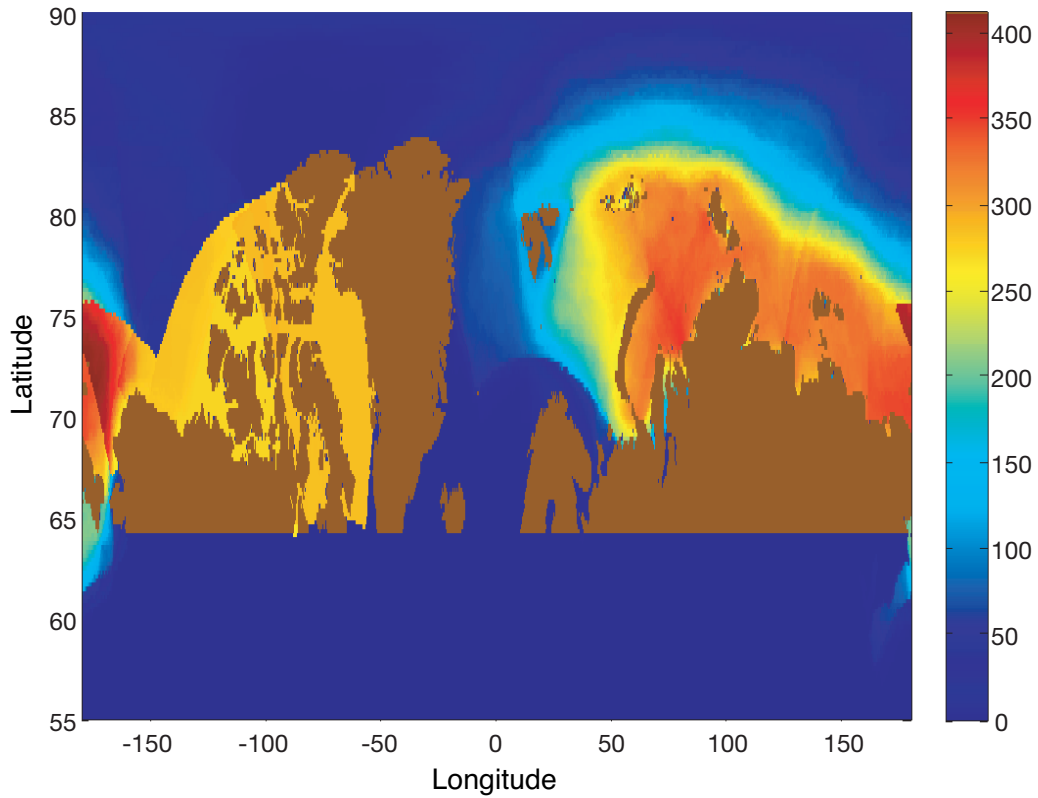


Figure 2.2: Number of valid data from 1953 - 1998 at each location after the interpolation steps. Maximum number of data is 411. Land area is shown in brown.

data location. Note that the actual data used here is altitude, so that the ocean depth values used in the study are negative numbers. When the average depth was less than 0, the location was assumed to be in the ocean. When the average depth was 0 or more, it was considered a land point. This definition can lead to sea ice occurring on land points, as an average depth above zero still permits

parts of the 0.2° square to be covered by ocean and thus contain sea ice at times.

The distance to the coastline was obtained by computing all great circle distances from any ocean point on the 0.2° grid to any point with altitude zero or higher of the 1' by 1' IBCAO data set. The minimum distance was taken as the distance to the coastline. The distance is measured as a solid angle in degrees. One degree corresponds to about 111 km.

Clearly, ocean depth and distance to nearest coastline are not independent from each other (see Figure 2.3). Indeed they correlate with an R^2 -coefficient of 0.51. We looked at both factors as it is not clear if it is rather the (shallow) depth of the ocean or the proximity of the (stabilizing) coast that facilitates the formation of landfast ice.

2.1.5 Wind Data

The NCEP/NCAR Reanalysis project is using a state-of-the-art analysis/forecast system to perform data assimilation using past data from 1948 to the present (Kalnay et al., 1996). We utilized monthly means of surface zonal and meridional wind as our wind data source. The NOAA Climate Diagnostics Center offers these data for free download as NetCDF files⁷. The spatial resolution of the data is 2.5° in longitude and latitude and thus much coarser than other data used in this analysis. To have wind data at each data location we used the

⁷<http://www.cdc.noaa.gov/>

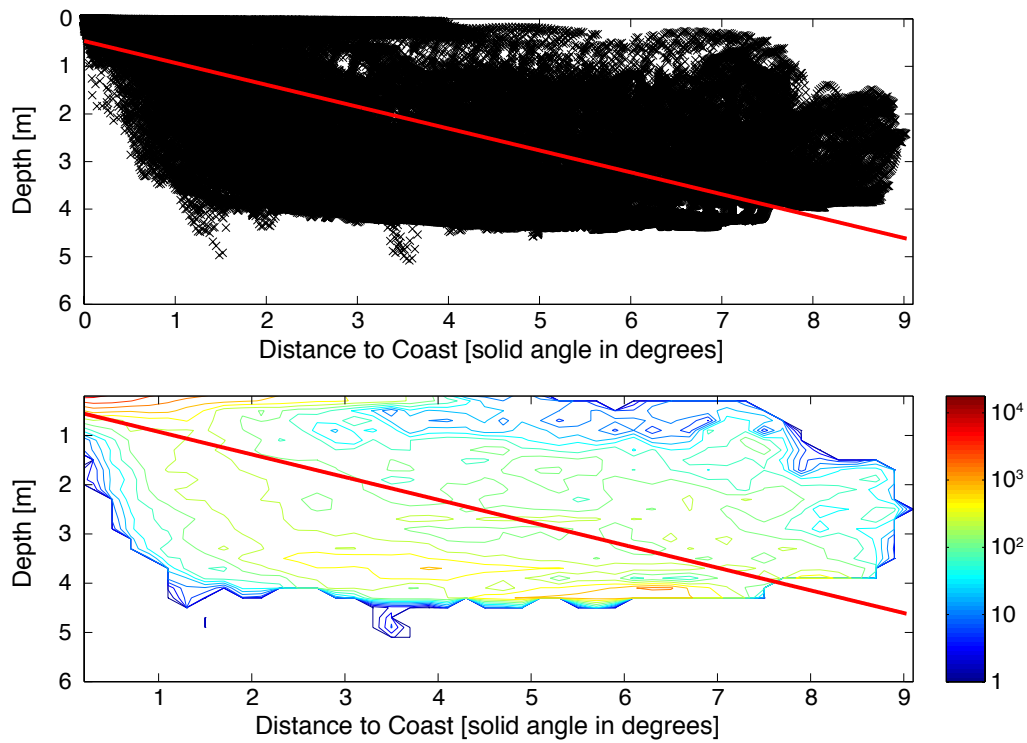


Figure 2.3: Scatter plot (top) and contour lines of data density (bottom) of ocean depths versus their distance to coast. Contour lines are shown every $10^{0.25}$. Data density is measured in number of data per 0.2 degrees distance and per 200 m depth. The red line shows the linear correlation between the two.

same wind information on a square of 2.5° by 2.5° around the actual wind data point. We preferred this method of simple distribution over other interpolation methods with the aim of adhering to the historical data and avoiding specious assumptions.

To find the strength of offshore winds, an offshore direction needed to be defined. For this we first created a landmask based on the IBCAO data by

setting each location to 0 (ocean) when the altitude was below zero and to 1 (land) whenever the altitude was zero or above. Then we took the negative gradient of this landmask using centered finite differences. To get an average offshore direction at each 0.2° data location, we averaged the gradient directions over a 0.2° square around the data location and normed this direction to unit length.

The wind vector from the data was then projected onto this offshore direction. The length of the projected vector became our offshore wind strength. Subtracting the offshore component from the wind vector also gave us the along-shore component for the statistical analysis.

2.2 Statistical Analysis

The landfast sea ice information was searched for correlations with respect to the following parameters:

- Ocean depth
- Distance to coast
- Monthly averaged winds (offshore and alongshore components)
- Long-term development

The data stems from a wide range of locations and spans over four decades, and we are not able to explain a significant part of the variance of the data, i.e. our correlation coefficients R^2 are normally very close to zero. Accordingly, we rather test if the β coefficient of the linear regression (i.e. the slope of the best-fitting line) is significantly different from zero at the 95% level, which implies that it is very likely that the factor looked at has an effect on landfast ice concentration. Figure 2.4 illustrates that point with January ice and wind data. That also means that the *beta* coefficients themselves (the slopes of the regression lines) have little meaning, what is relevant is that the 95% confidence interval excludes zero.

We primarily looked at all the data at once. In cases where no significant correlation was found, we were using data from individual months separately as well.

2.3 Results

2.3.1 Ocean depth

Linear regression of depth and landfast sea-ice concentration finds a statistically significant decline in landfast sea-ice concentration with increasing depths in the ocean (see Table 2.2). Remember, the actual parameter used in this regression

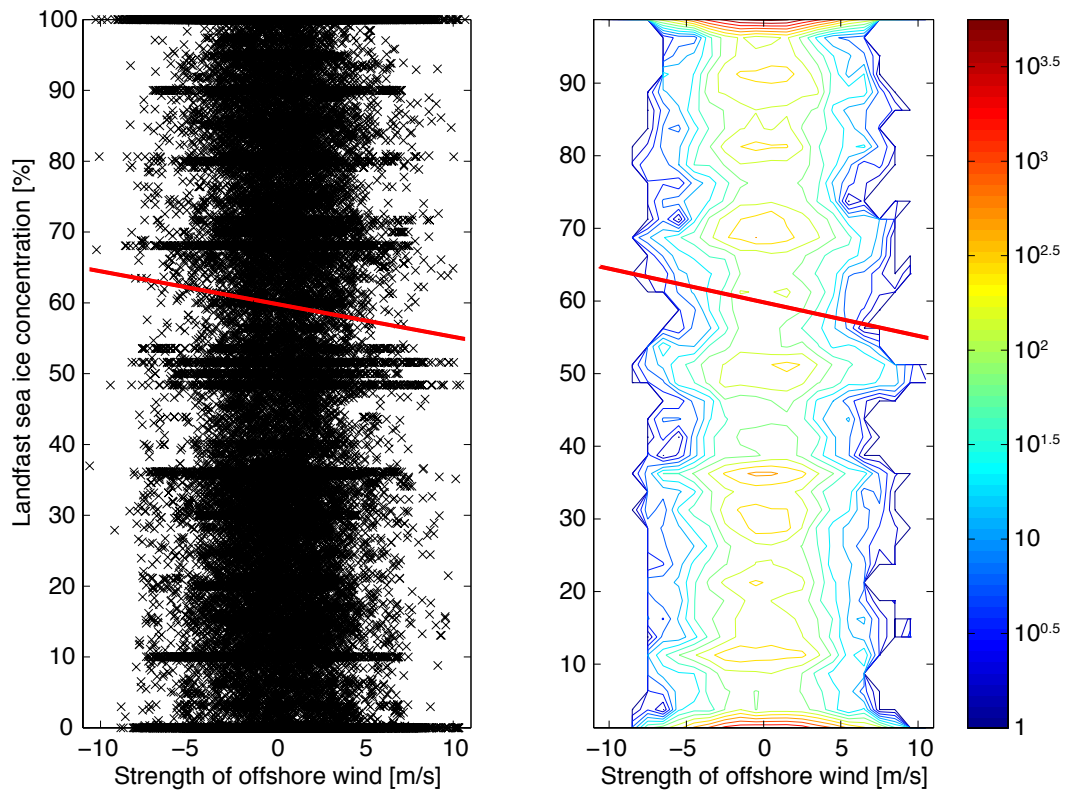


Figure 2.4: Scatter plot (left) and contour lines of the logarithm of data density (right) of offshore wind strengths versus landfast sea-ice concentrations for all January data. Contour lines are shown every $10^{0.25}$. Data density is measured in number of data per m/s and per 2.5% of landfast sea ice concentration. The red lines show the linear correlation between the two.

was elevation (i.e. negative depths), so that the positive β coefficient found actually implies that higher altitudes (and thus lower ocean depths) correlate with higher landfast ice concentrations.

Table 2.2: Correlations between topographical parameters and landfast sea-ice concentration.

Parameter	β coefficient and 95% confidence interval with units	
Depth	3.489 ± 0.0071	% lfi conc. ^a per km
Distance to coast	-3.317 ± 0.0053	% lfi conc. ^a per degree solid angle

^a “% lfi conc.” stands for “% landfast ice concentration”.

2.3.2 Distance to coast

The regression of distance to coast with landfast ice concentration gives a β coefficient that is significantly less than zero. This indicates that at greater distances from the coast less landfast sea ice is to be found, as is expected. This relationship is still significant but weakest from August to October (see Figure 2.5 for a month to month presentation).

2.3.3 Monthly averaged winds

For 9 out of 12 months, we find that stronger offshore winds go together with lower landfast sea-ice concentrations, as expected (see Figure 2.6). During three months (April, May and June) we cannot reject the null hypothesis that there is no effect of wind on landfast ice concentrations.

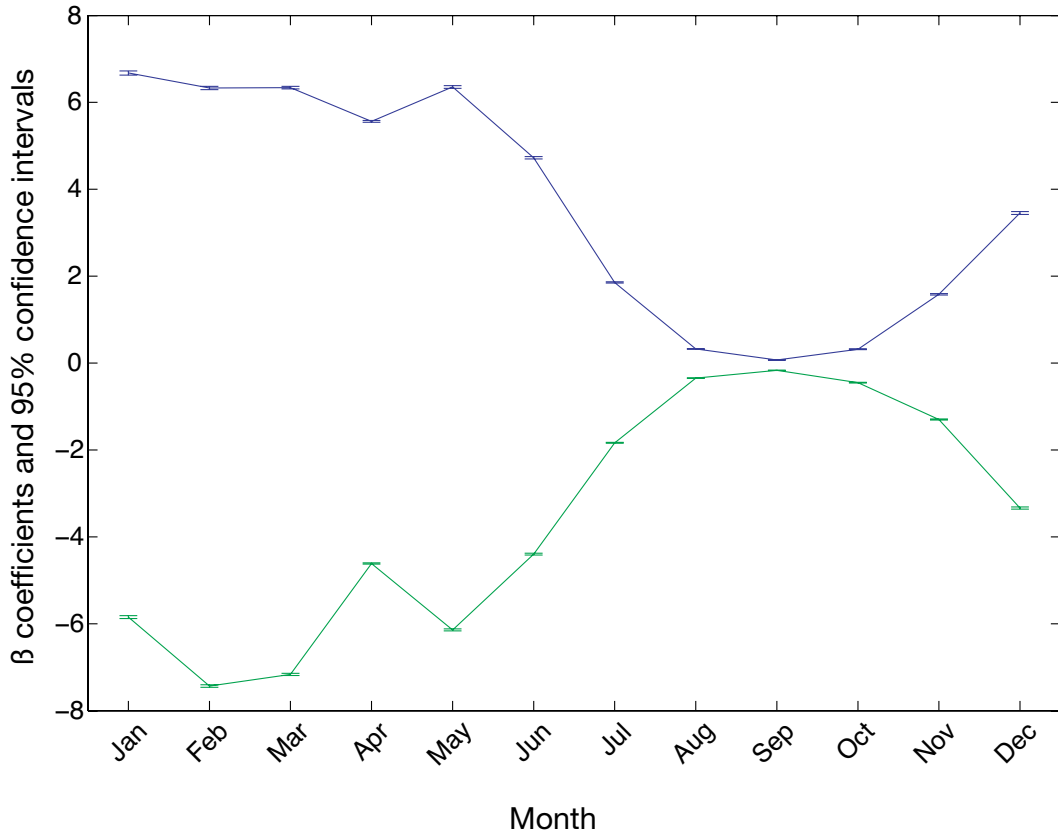


Figure 2.5: β coefficients of regressions of depth respective distance to coast versus landfast sea-ice concentration and their 95% confidence intervals. The upper curve shows the β coefficients with respect to ocean depth (in % landfast ice concentration per km), while the lower curve shows the β coefficients with respect to distance to coast (in % landfast ice concentration per degree solid angle).

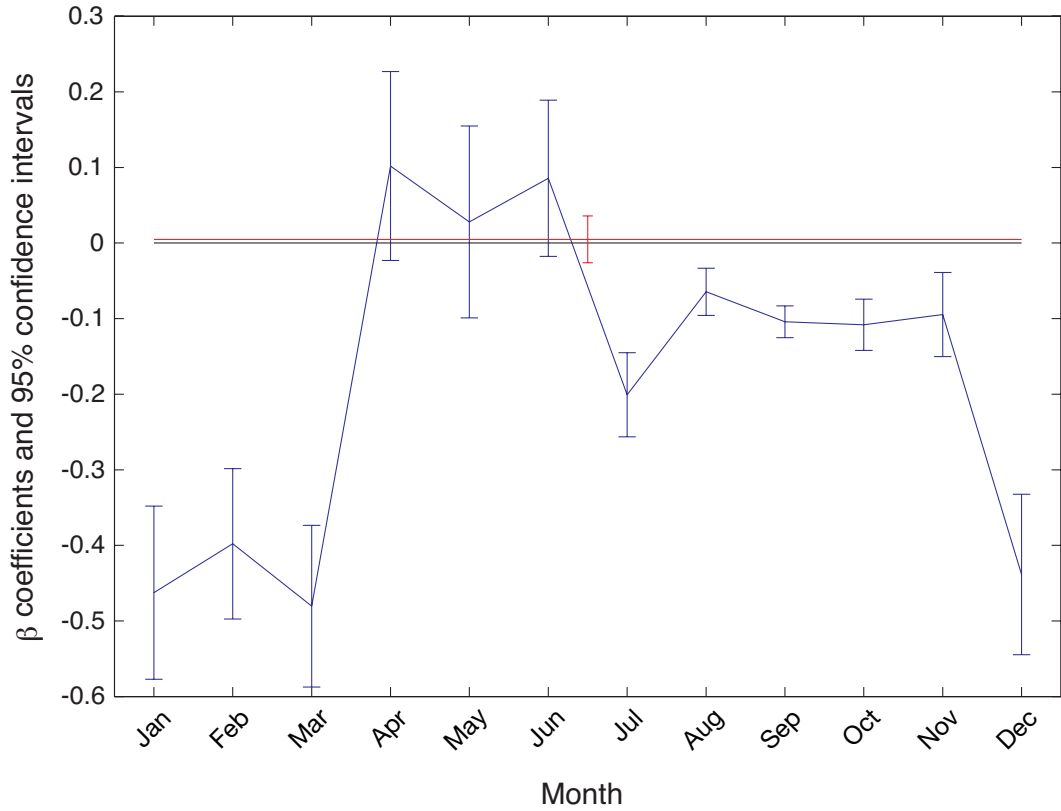


Figure 2.6: β coefficients of regressions of offshore wind strength versus landfast sea-ice concentration and their 95% confidence intervals (blue). From April to June the β coefficients are not significantly different from zero (black line). The β coefficient and 95% confidence interval of the regression using all data is shown in red.

2.3.4 Long-term Development

Regressions over time were done separately for each location. Figure 2.7 shows the regions where landfast ice has been decreasing (red), increasing (blue) or not changing significantly (yellow).

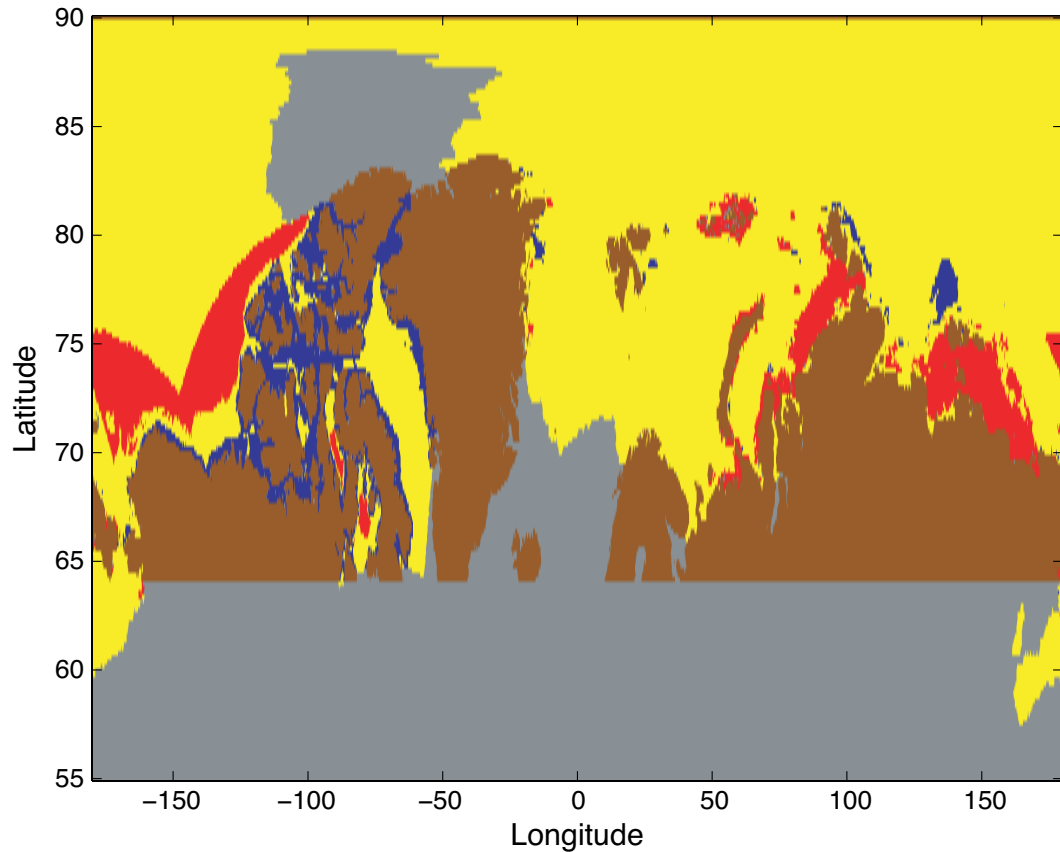


Figure 2.7: Significant changes of landfast sea-ice concentration over time. Red means a significant decrease and blue a significant increase in landfast ice concentration. Yellow signifies no significant change, while grey stands for missing data. Brown is land.

2.4 Discussion

2.4.1 Ocean Depth and Distance to Coast

Both ocean depth and distance to coastline significantly influence landfast ice concentration. This is not surprising in itself but has to our knowledge not been statistically shown before.

More interestingly, we find that landfast ice appears to larger depths than is often expected. Some authors suggested that landfast ice appears to ocean depths of about 18 meters (Wadhams, 1986) or to 20 meters (Barber and Hanesiak, 2004). Some models use similar parameterizations for landfast ice (Lieser, 2004). In our data we find that around 50% of landfast ice occurs on ocean depths deeper than 25 meters (see Figure 2.8). Considering this, alternative parameterizations should be developed.

Lastly, our data does not allow us to discriminate if ocean depth or distance to coast is a stronger influence on landfast ice.

2.4.2 Monthly averaged winds

We find that stronger offshore wind strengths go together with a decrease in landfast ice concentrations for nine out of twelve months. For three summer months (April to June), the effect is not significant.

We also looked at the effect of alongshore winds, and winds at 20° angles

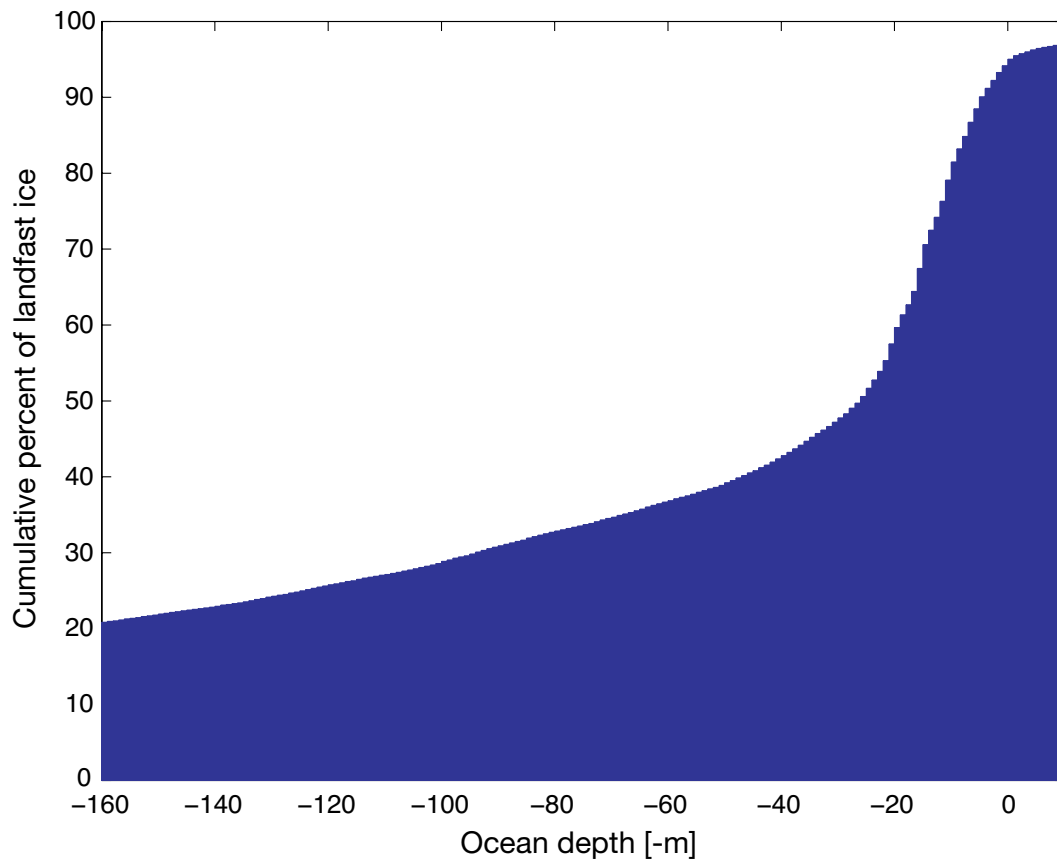


Figure 2.8: Percentage of landfast ice occurring at or below a certain depth. For example, 50% of landfast ice occurs at depths below 25 meters, or around 20% of landfast ice occurs on oceans deeper than 160 meters. This curve goes above a depth of zero because depths have been averaged over a 0.2 by 0.2° box.

on landfast ice (McPhee, 1975), but did not find any consistent or statistically significant influences.

2.4.3 Long-term Development

We find that from 1968 to 1990 there has been a significant decrease of landfast ice in the Beaufort and Chukchi Seas, along large parts of the Russian coast, around Novaya Zemlya and Franz Josef Land. There was an increase along most coasts of Northern Canada, the Canadian Archipelago, Western Greenland, Northern Severnaya Zemlya and North of the New Siberian Islands (see Figure 2.7).

Note that the sharp edge in the Beaufort and Chukchi Seas coincides with a change in amount of data available (see Figure 2.2). To the north of the line, data was much sparser.

Another source of error in this analysis is that it depends on the correct identification of landfast sea ice in the original data sets. Early Canadian ice charts, for example, seemed to call landfast ice often as “10/10” ice, i.e. as 100% sea ice rather than specifically identifying it as “landfast”. This might have introduced an artifactual increase of landfast sea ice within the Canadian Arctic. Indeed a recent study found a decrease in landfast sea ice thickness and duration in the Canadian Arctic (Dumas et al., 2006), which contradicts this

finding.

2.5 Data Acknowledgments

Sea-ice data was graciously provided by the “Canadian Ice Service” from “Environment Canada” on <http://ice-glaces.ec.gc.ca/app/WsvPageDsp.cfm?ID=11700>, as well as by the National Snow and Ice Data Center on <http://nsidc.org/>.

NCEP Reanalysis data for the monthly averaged winds was provided by the NOAA/OAR/ESRL PSD, Boulder, Colorado, USA, from their Web site at <http://www.cdc.noaa.gov/>.

Topographical data came from IBCAO on <http://www.ngdc.noaa.gov/mgg/bathymetry/arctic/> and had been converted to a 2-D NetCDF format by Ned Cokelet from NOAA/PMEL.

Chapter 3

Modeling

3.1 Introduction

A sea-ice dynamics model attempts to reproduce and predict the behavior of sea ice under the influence of atmosphere and ocean. Sea ice cannot be considered a passive tracer and assumptions about interactions of sea ice with itself have to be made (Coon, 1980, Hibler, 1979, Parkinson and Washington, 1979, see also section 1.3).

In this chapter I modify the de-facto standard viscous-plastic (VP) rheology introduced by Hibler (1977) as well as the elastic-viscous-plastic (EVP) rheology (Hunke and Dukowicz, 1997) in order to improve the representation of landfast sea ice in models.

Particularly the assumption of no tensile strength seems to break down in

the case of landfast ice. The data in the top right of Figure 2.5 for example shows data where landfast sea ice is present under the influence of strong offshore winds.

Several mechanisms could be causing sea ice to remain fast along the shoreline, for example shoals¹, grounded icebergs or islands that stabilize the ice (Divine et al., 2005).

But data shows that landfast ice also appears on depths that indicate that there is neither land close by nor that shallow water is an influence (see Figure 2.8) and thus I argue that another mechanism is needed, like the assumption that landfast ice contains a significant tensile strength.

Two predictable difficulties

At first glance, sea ice breaking under compression (for example when being pushed against a coast) seems symmetric to sea ice breaking under divergence (i.e. when being pulled apart by winds or currents). After some thought significant differences become readily apparent. When under compression, small fluctuations in ice thickness or concentration get smoothed out by further compression. This is because thinner areas of ice have relatively less strength and thus will be compressed more quickly than thicker areas, resulting in a homog-

¹Shoal: An area of shallow water, esp. as a navigational hazard. A submerged sandbank visible at low water (from The New Oxford American Dictionary).

enization of neighboring ice thicknesses.

In contrast, when sea ice is subjected to divergent stresses, small fluctuations lead to unstable behavior. If ice is even slightly thinner at one location, its relative weakness will lead to increased divergence, which in turn leads to it becoming even thinner. This makes the modeling of sea ice under divergent stresses (for example landfast sea ice under the influence of offshore winds) sensitive to numerical errors. A similar instability has been shown to exist in the regular viscous-plastic rheology even without diverging stresses Gray and Killworth (1995).

Even besides numerical considerations, the problem of predicting the break-off of landfast ice is ill-posed. Assume that a strip of landfast ice is subjected to increasing offshore winds. Initially, the tensile strength of the ice might be able to counteract the wind stress. But when winds keep increasing at some point the ice stress will exceed the maximum strength and will break apart.

Wherever the ice breaks it will reduce the total wind stress acting on the remaining landfast ice strip to values that again can be balanced by the tensile strength of the ice. The question remains how the location of breakage is being “chosen” by the real as well as the modeled sea ice and why.

Modeling assumptions

Sea ice normally appears in a wide variety of thicknesses, floe shapes, sizes and forms. To make modeling tractable I consider the ice to be a two-dimensional continuum (e.g. Gray and Morland, 1994, Hibler, 1980, Pritchard, 1975), which is the standard of sea ice modeling even though other methods have been used (Zyryanov et al., 2002, uses connected circular disks to model landfast ice). I further assume that two variables define the sea ice cover: the *ice concentration* a and the *equivalent ice thickness* h .

The ice concentration a is the fraction of the area in a grid cell covered by ice and thus will go from 0 to 1 (i.e. from 0% to 100%). Values of a below 1 imply that sub-grid-scale sized leads have opened so that $1 - a$ of the area is open ocean.

The equivalent ice thickness h measures the thickness that the total amount of ice in a grid cell would have were it spread out evenly. h is thus proportional to the total volume and total mass of ice in a grid cell but has a unit of length. The mass of sea ice in a cell is $\rho_i h \Delta x \Delta y$, where ρ_i is the density of sea ice, and Δx and Δy are the dimensions of the grid cell. This definition of h coincides with the definition used by Hibler (1979).

The average ice thickness, i.e. the mean thickness of ice in the area that actually is covered by ice, is h/a . Some authors (e.g. Hunke and Dukowicz,

1997) call this expression “ice thickness”, which should not be confused.

3.2 Momentum Equation

I use the following momentum equation:

$$m \frac{\partial \vec{u}}{\partial t} = -m f \vec{k} \times \vec{u} + \vec{\tau}_a + \vec{\tau}_o + \frac{\partial \sigma_{ij}}{\partial x_j} \quad (3.1)$$

The term on the left side stands for the change of momentum and contains the ice mass per unit area m as well as the acceleration of the ice. The non-linear advection term has been neglected as for example in Hunke and Dukowicz (1997) or Oberhuber (1993) but unlike many other studies (e.g. Hibler, 1979, Holland, 2006). There seems to be little agreement on the importance of this term, some studies ignore acceleration completely (e.g. Pritchard, 2001, Tremblay and Mysak, 1997).

The first term on the right side describes the Coriolis effect, with the Coriolis parameter f and the unit vector normal to the surface \vec{k} . $\vec{\tau}_a$ and $\vec{\tau}_o$ are atmosphere and ocean stresses. Finally $\frac{\partial \sigma_{ij}}{\partial x_j}$ is the divergence of the ice stress tensor; this term describes the forces stemming from ice interactions like rafting, ridging and fracturing (see section 1.3 for an introduction).

Hibler (1980) argues that based on observations as well as dimensional analysis those three terms on the right side dominate the momentum balance. Ocean surface tilt and current effects have been shown to be of smaller magnitude

than the other terms but can become significant over long time (Hibler, 1986). I ignore ocean effects in this study except for an ocean at rest to balance the wind stress.

Atmosphere and Ocean Stresses

Atmosphere and ocean stresses usually are of the following form:

$$\vec{\tau}_x = c_x \rho_x a |\vec{u}_x - \vec{u}| (\vec{u}_x - \vec{u}) \quad (3.2)$$

where a subscript x would be a “ a ” for the atmosphere or “ o ” for ocean stresses. ρ_a and ρ_o are the atmosphere respectively ocean densities, c_a and c_o the air and water drag coefficients (see Table 3.1 for the values used) and the wind, ocean current and ice velocities \vec{u}_a , \vec{u}_o and u . a is the ice concentration (area fraction) and needs to be included for two reasons. Firstly, the stresses have to go to zero if there is no ice in a grid cell (Gray and Morland, 1994), secondly without it the units are not identical to the other terms in the momentum equation (3.1), which only becomes obvious when remembering that a is a area fraction. Still many sources seem to forget to mention a (for example Flato and Hibler, 1992, Hibler, 1979, Hunke and Dukowicz, 1997, Tremblay and Mysak, 1997).

Sometimes turning angles are included in the wind or ocean stresses (McPhee, 1975) but are ignored here as landfast ice is not expected to move and more importantly for simplicity.

For the atmospheric stress I assume that wind velocities are much larger than ice velocities so that $\vec{u}_a \approx \vec{u}_a - \vec{u}$. The equation for the wind stress becomes

$$\vec{\tau}_a = c_a \rho_a a |\vec{u}_a| \vec{u}_a \quad (3.3)$$

Ocean effects are ignored here in this study except for a passive drag equivalent to the ice lying on top of an ocean at rest ($u_o \equiv 0$ at all times). This is necessary as otherwise ice would accelerate without limit under the influence of the atmospheric forcing as described above. The ocean drag term used in this model thus is

$$\vec{\tau}_o = -c_o \rho_o a |\vec{u}| \vec{u} \quad (3.4)$$

3.3 Modified Sea Ice Rheology

In the following I re-derive the viscous-plastic rheology introduced by (Hibler, 1979) allowing for tensile strength, i.e. resistance to divergence.

3.3.1 Moving the Elliptical Yield Curve

Unlike Hibler (1979) we allow for tensile strength, which means that the elliptical yield curve will reach into to the first quadrant (upper right part) of the principal stress diagram.

The maximum tensile stress that the ice can withstand is T and the maximal

compressive strength is P . Both numbers are assumed to be positive, i.e. P is positive for compressive strength while T is positive for tensile strengths.

The center of the ellipse is thus at $(-\frac{P-T}{2}, -\frac{P-T}{2})$. The eccentricity of the ellipse is e , which normally (and arbitrarily) is set to 2 (Hibler, 1979).

The semi-axes thus become $\frac{P+T}{2}\sqrt{2}$ and $\frac{P+T}{2e}\sqrt{2}$.

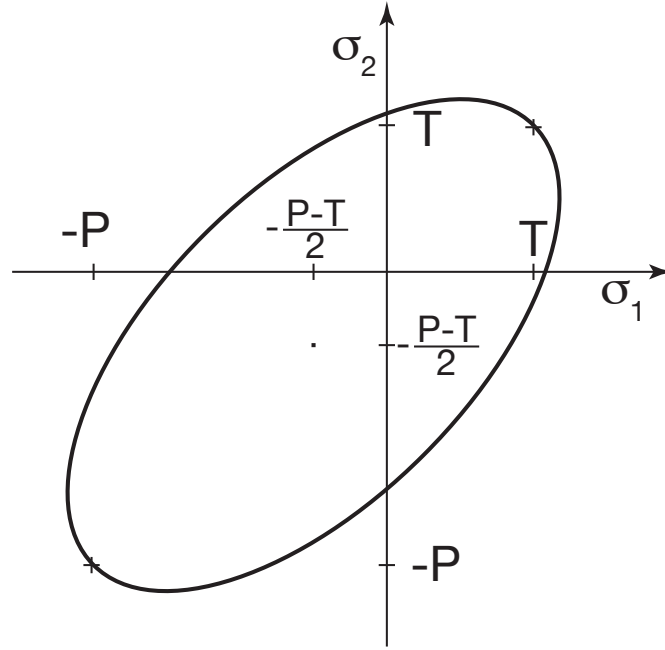


Figure 3.1: Relationship between the principal components of stress (σ_1 and σ_2) for a viscous-plastic rheology that allows for tensile strength.

The final equation for the moved elliptical yield curve then is:

$$F(\sigma_1, \sigma_2) = \left(\frac{\sigma_1 + \sigma_2 + P - T}{P + T} \right)^2 + \left(\frac{\sigma_1 - \sigma_2}{P + T} e \right)^2 - 1 = 0 \quad (3.5)$$

As suggested by Hibler (1979), P is generally set to

$$P = P^* h e^{-c^*(1-a)} \quad (3.6)$$

with the constants (Hunke and Dukowicz, 1997) as shown in Table 3.1.

Table 3.1: Constants and parameters used in the landfast sea ice model.

Symbol	Description	Value
c^*	Empirical ice strength parameter	20
c_a	Air drag coefficient	0.001
c_o	Ocean drag coefficient	0.004
Δ_{min}	Creep limit	$2 \cdot 10^{-9} \text{ s}^{-1}$
e	Yield curve axis ratio (eccentricity)	2
g	Gravitational acceleration	9.81
P^*	Empirical ice strength parameter	$27,500 \text{ N m}^{-1}$
ρ_a	Air density	1.3 kg m^{-3}
ρ_i	Ice density	900 kg m^{-3}
ρ_o	Ocean density	1025 kg m^{-3}

The ice thickness h and ice concentration a as introduced in section 3.4. I choose the tensile strength T to be proportional to P , which guarantees that the ellipse does not move relative to the origin with changing ice properties.

$$T = k_T P^* h e^{-c^*(1-a)} = k_T P \quad (3.7)$$

k_T is set to values in $[0, 1]$. Setting it to 0 recovers the regular ice rheology, while setting it to 1 assumes that ice can resist as much tension as it can compression. This would be realistic on a small scale (block of ice) but not on large scales where the ice is broken up into sub-grid-scale ice floes. Realistic geophysical values would thus probably be closer to 0 but that is the subject of future research.

Later we will need the equation of the elliptic yield curve to be with respect to the components of the stress tensor (σ_{11} , σ_{22} and $\sigma_{12} = \sigma_{21}$) rather than the principal stresses (σ_1 and σ_2), which are the eigenvalues of the stress tensor (see introduction). After a change of variables the same equation looks as follows:

$$F(\sigma_{11}, \sigma_{22}, \sigma_{12}, \sigma_{21}) = \left(\frac{\sigma_{11} + \sigma_{22} + P - T}{P + T} \right)^2 + \frac{e^2 [(\sigma_{11} - \sigma_{22})^2 + 4\sigma_{12}\sigma_{21}]}{(P + T)^2} - 1 = 0 \quad (3.8)$$

3.3.2 New Constitutive Law

We assume the ice to obey the two-dimensional constitutive law

$$\sigma_{ij} = 2\eta\dot{\epsilon}_{ij} + (\zeta - \eta)(\dot{\epsilon}_{11} + \dot{\epsilon}_{22})\delta_{ij} - \frac{P}{2}\delta_{ij} \quad (3.9)$$

where σ_{ij} is the stress tensor, $\dot{\epsilon}_{ij}$ is the strain rate tensor, $P/2$ is a pressure term that depends on the local ice properties, and ζ and η are bulk and shear viscosities that depend on P as well as $\dot{\epsilon}_{ij}$.

In the following, we will often look at the constitutive law solved for the strain rates. Inverting equation (3.9) we get

$$\dot{\epsilon}_{ij} = \frac{1}{2\eta}\sigma_{ij} + \frac{\eta - \zeta}{4\eta\zeta}(\sigma_{11} + \sigma_{22})\delta_{ij} + \frac{P}{4\zeta}\delta_{ij} \quad (3.10)$$

Assuming a normal flow rule (Goodier and Hodge, 1958) we assume that the ice breaks in the direction where the stress is reaching the yield curve, i.e.

$$\dot{\epsilon}_{ij} = \gamma \frac{\partial F}{\partial \sigma_{ij}} \quad (3.11)$$

where F had been defined in equation (3.5) and γ is a proportionality constant about to be defined below.

Taking all the partial derivatives of F with respect to σ_{ij} we find the following dependence of the strain rate tensor $\dot{\epsilon}_{ij}$ from the stress tensor σ_{ij} :

$$\dot{\epsilon}_{ij} = \gamma \left[\frac{4e^2}{(P+T)^2}\sigma_{ij} + \frac{2(1-e^2)}{(P+T)^2}(\sigma_{11} + \sigma_{22})\delta_{ij} + \frac{2(P-T)}{(P+T)^2}\delta_{ij} \right] \quad (3.12)$$

Solving this for all σ_{ij} and re-substituting them into (3.5) we find γ as follows

$$\gamma = \frac{P+T}{4} \sqrt{(\dot{\epsilon}_{11}^2 + \dot{\epsilon}_{22}^2)(1+e^{-2}) + \frac{4}{e^2}\dot{\epsilon}_{12}^2 + 2\dot{\epsilon}_{11}\dot{\epsilon}_{22}(1-e^{-2})} = \frac{P+T}{4}\Delta \quad (3.13)$$

where Δ is being introduced for brevity.

Combining (3.12) and (3.13) we get the dependence of the strain rate from the internal ice stresses assuming an elliptical yield curve.

$$\dot{\epsilon}_{ij} = \frac{\Delta}{2} \left[\frac{2e^2}{P+T}\sigma_{ij} + \frac{1-e^2}{P+T}(\sigma_{11} + \sigma_{22})\delta_{ij} + \frac{P-T}{P+T}\delta_{ij} \right] \quad (3.14)$$

Comparing this to the general constitutive law (3.9) we see that all the terms line up nicely and thus we can define bulk and shear viscosities as follows

$$\zeta = \frac{P + T}{2\Delta} \quad \text{bulk viscosity} \quad (3.15)$$

$$\eta = \frac{P + T}{2\Delta e^2} = \frac{\zeta}{e^2} \quad \text{shear viscosity} \quad (3.16)$$

Small strain rates can make Δ arbitrarily small, letting the viscosities become infinite. Hibler (1979) regularized this behavior by bounding them by the large values $\zeta_{max} = 2.5 \cdot 10^8 P \text{ g s}^{-1}$ and $\eta_{max} = \frac{\zeta_{max}}{e^2}$. This is equivalent to bounding Δ by a minimal value of $\Delta_{min} = 2 \cdot 10^{-9} \text{ s}^{-1}$, which is what I will do from here on.

Remark to the derivation of the constitutive law

As we know from the beginning that $\sigma_{12} = \sigma_{21}^2$ and thus that $\sigma_{21} = \sigma_{21}(\sigma_{12})$ is a function of σ_{12} and vice versa, the chain rule needs to be applied when taking derivatives with respect to σ_{12} . In particular the derivative of the term with σ_{12} and σ_{21} in (3.8) has traditionally (Hibler, 1979, Hunke and Dukowicz, 1997) been evaluated as follows.

$$\frac{\partial 4\sigma_{12}\sigma_{21}}{\partial \sigma_{12}} = 4\sigma_{21} \quad \text{and} \quad \frac{\partial 4\sigma_{12}\sigma_{21}}{\partial \sigma_{21}} = 4\sigma_{12} \quad (3.17)$$

²This is true except for cases where a torque is being applied to the bulk of an arbitrary fluid parcel and not only to its surface. An example for such an exception would be a medium consisting of a suspension of ferromagnetic particles, each being subject to the torque of an applied magnetic field (Acheson, 1990).

which become $4\sigma_{12}$ after setting $\sigma_{12} = \sigma_{21}$.

But keeping in mind that $\sigma_{21} = \sigma_{21}(\sigma_{12})$ and thus using the chain rule one gets:

$$\begin{aligned} \frac{\partial 4\sigma_{12}\sigma_{21}(\sigma_{12})}{\partial \sigma_{12}} &= \frac{d 4\sigma_{12}\sigma_{21}(\sigma_{12})}{d\sigma_{12}} + \frac{d 4\sigma_{12}\sigma_{21}(\sigma_{12})}{d\sigma_{21}} \cdot \frac{d\sigma_{21}(\sigma_{12})}{d\sigma_{21}} \\ &= 4\sigma_{21} + 4\sigma_{12} \cdot 1 \\ &= 8\sigma_{12} \end{aligned} \tag{3.18}$$

after setting $\sigma_{21} = \sigma_{12}$, which is a factor of two different from the result obtained above.

The derivative with respect to σ_{21} can be taken analogously with the same result.

Another way of showing the correctness of the second result is by setting $\sigma_{21} = \sigma_{12}$ from the beginning. Then the one derivative becomes

$$\frac{\partial 4\sigma_{12}\sigma_{21}(\sigma_{12})}{\partial \sigma_{12}} = \frac{\partial 4\sigma_{12}^2}{\partial \sigma_{12}} = 8\sigma_{12} \tag{3.19}$$

confirming the result obtained from using the chain rule.

3.3.3 Adding Elasticity

One way to numerically solve the equations presented so far is to add an elastic term, as was proposed by Hunke and Dukowicz (1997). The constitutive

equations (3.10) then turn into

$$\dot{\epsilon}_{ij} = \underbrace{\frac{1}{E} \frac{\partial \sigma_{ij}}{\partial t}}_{\text{elastic term}} + \underbrace{\frac{1}{2\eta} \sigma_{ij} + \frac{\eta - \zeta}{4\eta\zeta} (\sigma_{11} + \sigma_{22}) \delta_{ij} + \frac{P}{4\zeta} \delta_{ij}}_{\text{viscous-plastic rheology}} \quad (3.20)$$

E corresponds to Young's modulus. While sea ice certainly has a certain elasticity and such a term makes physical sense physically (Colony and Pritchard, 1975, Coon et al., 1974, Holland, 2006, Pritchard, 2001, 1975), the values of E used here are purely motivated by its numerical effect and have nothing to do with the elastic property of sea ice. Still the modifications assume a new elastic-viscous-plastic (EVP) rheology of sea ice, and the physical implications are significant.

The addition of an elasticity turns our modeled sea ice into a *Maxwell material* as long as we remain within the yield curve and no plastic deformation takes place. A Maxwell material can be thought of as a viscous damper connected in series to an elastic spring (see Figure 3.2.

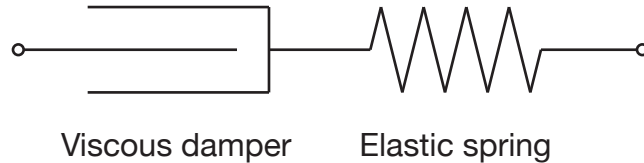


Figure 3.2: Idealized schematic of a Maxwell material.

If a stress is added, the elastic element immediately deforms while the viscous element deforms at a constant rate. Upon release of the stress, the elastic

element springs back to its original position while the deformation of the viscous element remains unchanged. This slow viscous deformation is also called *creep*.

The motivation behind adding the elastic term is that the time derivative of the stresses will go to zero over time (during which the forcing will remain constant). Once the elastic term has approached zero, equation (3.20) becomes the original viscous-plastic constitution law and we recovered the desired solution. The Young's modulus has thus to be chosen in a way that any elastic waves have enough time to die away before the forcings and other variables are updated.

Adding this time derivative also has the effect that there is now a time derivative in the stress equation, so that explicit methods can be used. The viscous-plastic rheology (3.9) itself is elliptical in nature and thus has to be solved with more expensive implicit methods.

In areas of slow ice movements, the viscosities can grow very large, forcing the time steps to become very small. The introduction of the elasticity alleviates this situation and allows much bigger time steps. A detailed analysis of that is given in Hunke and Dukowicz (1997). This can be seen somewhat more intuitively when solving for the time derivative of the stress tensor and multiplying the whole equation by Young's modulus E :

$$\frac{\partial \sigma_{ij}}{\partial t} = E \dot{\epsilon}_{ij} + \frac{E}{2\eta} \sigma_{ij} - \frac{E(\eta - \zeta)}{4\eta\zeta} (\sigma_{11} + \sigma_{22}) \delta_{ij} - \frac{EP}{4\zeta} \delta_{ij} \quad (3.21)$$

Wherever there is a viscosity in the denominator, Young's modulus E counteracts it thus easing the restriction on the time step.

3.4 Conservation Laws

From our definitions of the ice concentration a and equivalent ice thickness h it becomes clear that the following conditions have to be fulfilled at all times

$$0 \leq a \leq 1 \tag{3.22}$$

$$0 \leq h \tag{3.23}$$

In our simplified model, we will assume that we have no freezing or melting, i.e. we want the total mass of sea ice to remain conserved. As we assume the ice density to be constant, this is equivalent to assuming ice volume conservation.

$$\frac{\partial h}{\partial t} + \nabla(\vec{u} \cdot h) = 0 \tag{3.24}$$

Additionally, we want the actual average ice thickness h/a to remain constant with the flow. The only times when ice shall become thicker is when it gets compressed strongly enough to start to fracture and form ridges. Thus we want

$$\frac{DH}{Dt} = 0 \tag{3.25}$$

or

$$\frac{\partial H}{\partial t} + \vec{u} \cdot \nabla H = 0 \tag{3.26}$$

where I use $H = h/a$ for simplicity.

From the mass conservation equation (3.24) we know (using $h = Ha$ and the multiplication rule, and rearranging):

$$\frac{\partial Ha}{\partial t} + \vec{u} \cdot \nabla (Ha) + Ha \nabla \cdot \vec{u} = 0 \quad (3.27)$$

$$H \frac{\partial a}{\partial t} + a \frac{\partial H}{\partial t} + \vec{u} H \cdot \nabla a + \vec{u} a \cdot \nabla H + Ha \nabla \cdot \vec{u} = 0 \quad (3.28)$$

$$H \left(\frac{\partial a}{\partial t} + \vec{u} \cdot \nabla a + a \nabla \cdot \vec{u} \right) + a \underbrace{\left(\frac{\partial H}{\partial t} + \vec{u} \cdot \nabla H \right)}_{=0 \text{ (equation 3.26)}} = 0 \quad (3.29)$$

If $H = 0$ there is no ice and the last equation is trivially true. If there is ice, then

$$\frac{\partial a}{\partial t} + \nabla(\vec{u} \cdot a) = 0 \quad (3.30)$$

which is equivalent to a conservation of ice concentration a , which can be easily implemented, analogous to the mass conservation (3.24).

As the ice concentration a is restricted to $[0, 1]$ it is not truly conserved. Once 1 has been reached in a convergent situation, a remains there while the mass continues to increase. In such a case the average ice thickness h/a is increasing too, i.e. the ice is being crushed and getting thicker, which is the desired behavior.

3.5 One-dimensional Numerical Implementation

3.5.1 The One-dimensional Equations

I implement a one-dimensional model to get an impression of the behavior. Most variables retain their meaning, of note is the stress tensor that turns into a single stress variable σ which corresponds to σ_{11} of the two-dimensional case, i.e. stress in the x -direction applied to a surface pointing into the x -direction.

As compared to the momentum equation (3.1) I ignore the Coriolis force, which has no effect in a purely one-dimensional system. All I want to retain is the ice rheology and one forcing term, in this case wind stress, to isolate the effects of my changes in the sea-ice rheology on the creation and maintenance of landfast sea ice. The ocean drag becomes necessary as a restoring drag as with wind forcing alone, ice velocities can grow without limit.

The one-dimensional momentum conservation becomes

$$m \frac{\partial u}{\partial t} = \frac{\partial \sigma}{\partial x} + \tau_a + \tau_o \quad (3.31)$$

Atmosphere and ocean stresses retains their definitions from equations (3.3) and (3.4) except that only one component of the velocity vectors is left. Still the ocean is at rest so that the ocean drag always tries to restore ice velocities to zero.

$$\tau_a = c_a \rho_a a |u_a| u_a \quad (3.32)$$

$$\tau_o = -c_o \rho_o a |u| u \quad (3.33)$$

There is no shear stress in one dimension and any derivatives with respect to y vanish. The elliptical yield curve collapses to a line. The one-dimensional constitutive law is found by letting the eccentricity e of the yield curve go to ∞ and setting $\dot{\epsilon}_{22}$ and $\dot{\epsilon}_{12}$ to zero. This lets the shear viscosity in (3.16) go to zero as desired.

The constitutive law (3.9), i.e. the equation for the stress σ becomes

$$\sigma = \zeta \frac{\partial u}{\partial x} - \frac{P - T}{2} = \frac{P + T}{2\Delta} \frac{\partial u}{\partial x} - \frac{P - T}{2} \quad (3.34)$$

where the bulk viscosity $\zeta = \frac{P+T}{2\Delta}$, the compressive strength P and the tensile strength $T = k_T P$ are defined identically to the two-dimensional case. Δ from equation (3.13) simplifies considerably to become

$$\Delta = \max \left(\Delta_{min}, \left| \frac{\partial u}{\partial x} \right| \right) \quad (3.35)$$

Note that except for very small strain rates the first term of the right side of equation (3.34) contains the fraction $\frac{\partial u}{\partial x} / |\frac{\partial u}{\partial x}|$, which is just the sign of the strain rate, $\text{sgn} \left(\frac{\partial u}{\partial x} \right)$. This represents the desired plastic behavior. Under convergence, $\frac{\partial u}{\partial x}$ is negative and the stress σ becomes $-P$, the critical stress under convergence (note that compressive stresses have a negative sign). Under divergence on the other hand, the stress σ goes up to at most T , again as desired.

In between, i.e. for $|\frac{\partial u}{\partial x}| < \Delta_{min}$, the stresses vary between those two values, linearly depending on the strain rate, enabling the ice to resist pressure or

tension through the creation of small strain rates. While resisting those forces, the ice experiences a slow creep of Δ_{min} that is assumed to be slow enough to be negligible on geophysical time scales. See Figure 3.3 for an illustration of the behavior just described.

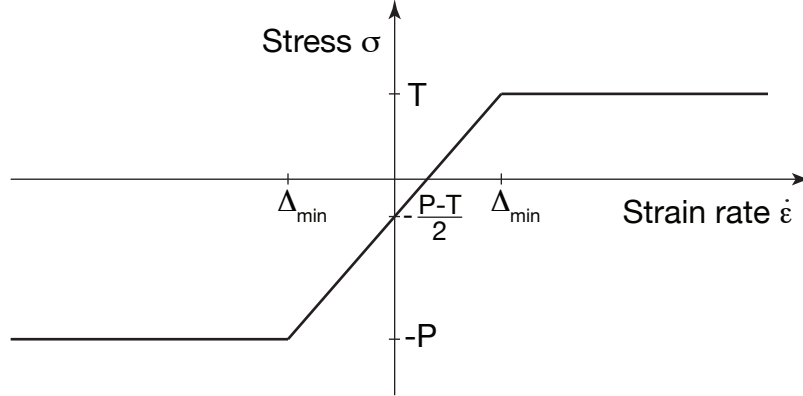


Figure 3.3: One-dimensional stress-strain rate diagram for a viscous-plastic material.

Besides conserving momentum (3.31) while satisfying the constitutive law (3.34), we also have to conserve the equivalent ice thickness h and the ice concentration a and keep the latter within $[0, 1]$. The respective equations (3.24), (3.30) and (3.22) simplify in one dimension to:

$$\frac{\partial h}{\partial t} + \frac{\partial(uh)}{\partial x} = 0 \quad (3.36)$$

$$\frac{\partial a}{\partial t} + \frac{\partial(ua)}{\partial x} = 0 \quad (3.37)$$

where $0 \leq a \leq 1$

This provides us with the necessary four equations to solve for the four

unknowns u , σ , h and a .

3.5.2 Discretizations

As $\frac{\partial u}{\partial t}$ depends on $\frac{\partial \sigma}{\partial x}$ and σ depends on $\frac{\partial u}{\partial x}$ one cannot help but think of a staggered grid. Ice stress, thickness and concentration are defined at one set of grid points (the *material points*) while ice velocities are defined in between and to the left and right (see Figure 3.4) on the *velocity points*. This leads to there being one more velocity point than there are material points.

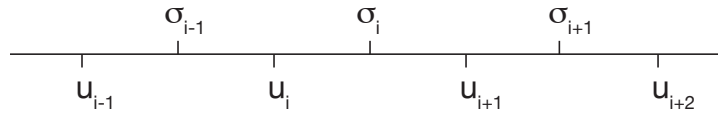


Figure 3.4: The staggered grid used in the one-dimensional model. u 's denote velocity points, while σ 's label material points, at which the equivalent ice thickness h and ice concentration a are also defined.

The ice rheology strictly speaking is part of the momentum equation so the two equations are solved together. I used two methods to solve them, on the one hand solving the viscous-plastic (VP) rheology with an implicit scheme, on the other hand I used the elastic-viscous-plastic (EVP) rheology to solve them. In the one-dimensional case speed is not really an issue, and both methods actually execute in about the same time. Further, this allows a comparison between the viscous-plastic and the elastic-viscous-plastic rheologies.

Solving the momentum equation implicitly

The momentum equation will be solved on the velocity points. For this purpose for example the equivalent ice thickness, which is defined at the material points, will have to be interpolated (i.e. averaged) onto the velocity points. I will denote such interpolation with a superscripted u on the left side of the variable; ${}^u h$ for example is the equivalent ice thickness at velocity points.

Subscripts i to the right indicate the location of a variable, i.e. the grid index. Note that the actual location of a variable with subscript i depends on the variable (see Figure 3.4). The exception to this rule is ρ_i , the density of sea ice, where the i stands for “ice”.

Superscripts to the right indicate at which time (index) the value lies. The current (known) time level is indicated with a superscript of k , the next time step is at $k + 1$.

I use simple first-order differences in space as well as in time (e.g. Durran, 1999), so that the momentum equation (3.31) becomes

$$\rho_i {}^u h_i^k \frac{u_i^{k+1} - u_i^k}{\Delta t} = \frac{\sigma_i^{k+1} - \sigma_{i-1}^{k+1}}{\Delta x} + \tau_a^k - c_o \rho_o {}^u a_i^k |u_i^k| u_i^{k+1} \quad (3.38)$$

where I keep on using $\tau_a^k = c_a \rho_a {}^u a^k |u_a^k| u_a^k$ for brevity as it is a purely external forcing term.

The discretized constitutive law (3.34) is

$$\sigma_i^{k+1} = \frac{1 + k_T}{2} P_i^k \frac{u_{i+1}^{k+1} - u_i^{k+1}}{\Delta x \Delta_i^k} - \frac{1 - k_T}{2} P_i^k \quad (3.39)$$

It helps to introduce some shortcuts:

$$\begin{aligned}
k^+ &= \frac{1 + k_T}{2\Delta x} \\
k^- &= \frac{1 - k_T}{2\Delta x} \\
\Delta_i^{*k} &= \Delta x \Delta_i^k = \Delta x \max\left(\Delta_{min}, \frac{|u_{i+1}^k - u_i^k|}{\Delta x}\right) \\
&= \max\left(\Delta x \Delta_{min}, |u_{i+1}^k - u_i^k|\right) \\
&= \max\left(\Delta_{min}^*, |u_{i+1}^k - u_i^k|\right)
\end{aligned}$$

where $\Delta_{min}^* = \Delta x \cdot 2 \cdot 10^{-9} \text{m s}^{-1}$ and $P_i^k = P^* h_i^k e^{-c^*(1-a_i^k)}$. Inclusion of Δx in k^+ and k^- is motivated by the fact that we need the x -derivative of σ for the momentum equation and thus will be able to take care of the Δx 's coming from there. The discretized constitutive law looks as follows after using the shortcuts:

$$\sigma_i^{k+1} = \Delta x k^+ P_i^k \frac{u_{i+1}^{k+1} - u_i^{k+1}}{\Delta_i^{*k}} - \Delta x k^- P_i^k \quad (3.40)$$

Now we are ready to substitute the expression for σ into the discretized momentum equation and sort the terms by the different u -terms:

$$\begin{aligned}
&u_{i-1}^{k+1} \left(-k^+ \frac{P_{i-1}^k}{\Delta_{i-1}^{*k}}\right) \\
&+ u_i^{k+1} \left(\frac{\rho_i u_i^k}{\Delta t} + k^+ \left(\frac{P_{i-1}^k}{\Delta_{i-1}^{*k}} + \frac{P_i^k}{\Delta_{i-1}^{*k}}\right) + c_o \rho_o u_i^k |u_i^k|\right) \\
&+ u_{i+1}^{k+1} \left(-k^+ \frac{P_i^k}{\Delta_{i-1}^{*k}}\right) \\
&= \frac{\rho_i u_i^k}{\Delta t} u_i^k - k^- (P_i^k - P_{i-1}^k) + \tau_a \quad (3.41)
\end{aligned}$$

The right hand side is completely known at time k , and so are the factors

behind the new velocities u^{k+1} , so that the equations for all grid points can be written as

$$A^k u^{k+1} = b^k$$

where A is a tridiagonal matrix.

Before we can solve for u^{k+1} , A needs to contain information about the boundary conditions. I implemented two different boundary conditions, “closed” and “open”. Closed boundaries are like walls and stop ice that moves against it. The velocities along a closed boundary are all set and kept to zero (Dirichlet boundary condition). Open boundaries allow sea ice to leave the modeled domain. This is being implemented by enforcing zero derivatives at the boundaries (Neumann boundary condition), respectively setting velocities on the boundary equal to the velocities just inside the domain in the numerical implementation.

For closed boundaries in the implicit code I set u_1^{k+1} as well as $u_{n_x+1}^{k+1}$ to zero at all times (n_x is the number of spatial grid points). That means that the respective terms on the left hand side of (3.41) will fall away.

For open boundaries, we demand that $u_1^{k+1} = u_2^{k+1}$ (and analogously on the other border). For $i = 2$ for example the momentum equation becomes

$$\begin{aligned} & u_2^{k+1} \left(-k + \frac{P_1^k}{\Delta_1^{*k}} \right) \\ & + u_2^{k+1} \left(\frac{\rho_i u_2^k h_2^k}{\Delta t} + k + \left(\frac{P_1^k}{\Delta_1^{*k}} + \frac{P_2^k}{\Delta_2^{*k}} \right) + c_o \rho_o u_i^k |u_2^k| \right) \\ & + u_3^{k+1} \left(-k + \frac{P_2^k}{\Delta_2^{*k}} \right) \end{aligned}$$

$$= \frac{\rho_i u h_2^k}{\Delta t} u_2^k - k^- (P_2^k - P_1^k) + \tau_a \quad (3.42)$$

which simplifies to

$$\begin{aligned} u_2^{k+1} \left(\frac{\rho_i u h_2^k}{\Delta t} + k^+ \frac{P_2^k}{\Delta_{*k}^k} + c_o \rho_o u a_i^k |u_2^k| \right) + u_3^{k+1} \left(-k^+ \frac{P_2^k}{\Delta_{*k}^k} \right) \\ = \frac{\rho_i u h_2^k}{\Delta t} u_2^k - k^- (P_2^k - P_1^k) + \tau_a \end{aligned} \quad (3.43)$$

After adjusting A for the boundaries, $u^{k+1} = A^{k-1} b^k$ is iterated with updating A and b in between until the changes in the 2-norm of u are less than 10^{-6} . Both that value as well the choice of the 2-norm are somewhat arbitrary but seem to be appropriate.

Conservation of equivalent ice thickness and ice concentration

Having solved the momentum equations, ice mass and concentration conservation have to be taken care of. A natural way to achieve this is to evaluate the flux at each cell interface and then difference those fluxes across each cell (Durrant, 1999). The staggered grid simplifies this process as the velocities are already given between the material cells so that there is no need for averaging or interpolation.

To find a flux between two cells, we want to know how fast ice is moving between the cells and multiply this by the amount of conserved quantity from where the velocity is coming from. One way to formulate this is as follows

(shown at the example of the equivalent ice thickness h):

$$fl_i = \frac{u_i}{2}(h_{i-1} + h_i) + \frac{|u_i|}{2}(h_{i-1} - h_i) \quad (3.44)$$

and equivalently for the ice concentration. fl is the flux at the velocity grid point indexed with i . This velocity point lies between the material points indexed with $i - 1$ and i (see Figure 3.4). If u_i is positive, the flux becomes $u_i h_{i-1}$, if negative it is $u_i h_i$, as desired.

A conserved quantity is updated as follows:

$$h_i^{k+1} = h + i^k + \frac{\Delta t}{\Delta x}(fl_i - fl_{i+1}) \quad (3.45)$$

which is the discretized version of (3.36) using simple differences. (3.37) has been implemented accordingly.

After this step, wherever the ice concentration should have become bigger than 1, it is reset to 1.

Both variables are set to 10^{-6} should they have decreased below that value. This is to prevent the ice mass in a grid cell from approaching zero too closely as the momentum equation is not defined with no ice mass. This is standard procedure, other implementations of sea ice models that I have heard of use a minimal thickness and concentration of 10^{-3} , but it does violate mass conservation to a small degree.

Solving the equations using the elastic-viscous-plastic rheology

To discretize the elastic-viscous-plastic constitution law (3.20) introduced in section 3.3.3, I solve for the time derivative and multiply by Young's modulus E . The viscosities are substituted by their viscous-plastic definitions (3.15) and (3.16).

$$\frac{\partial \sigma}{\partial t} = E \frac{\partial u}{\partial x} - \frac{2E}{P+T} \cdot \Delta \cdot \sigma - \frac{E(P-T)}{P+T} \cdot \Delta \quad (3.46)$$

P , T and Δ retain their meaning from earlier. The Young's modulus E is defined as $2E_0\rho_i h_i (\Delta x/\Delta t_e)^2$ (Hunke and Dukowicz, 1997) with E_0 an elasticity parameter that should be chosen between 0 and 1 (see Table 3.2). Δt_e is the elastic time step, which is N times smaller than the advective time step. The advective time step is identical to the time step used in the implicit scheme described above. Only every advective time step the ice thickness and concentration and thus the viscosities that depend on them are updated.

N can be chosen freely and corresponds to the number of iterations that the momentum and rheology equations are computed before the other variables are updated. Hunke and Dukowicz (1997) used values from 72 to 400 for N , a typical value for N that I used is 250.

Again using simple differencing on the staggered grid, the discretized equation for the internal ice stress is

$$\sigma_i^{k+1} - \sigma_i^k = E\Delta t_e \frac{u_{i+1}^k - u_i^k}{\Delta x} - \frac{2E\Delta t_e}{(1+k_T)P} \cdot \Delta_i^k \cdot \sigma_i^{k+1} - \frac{1-k_T}{1+k_T} E\Delta t_e \cdot \Delta_i^k \quad (3.47)$$

Not that for increased stability, the σ on the right hand side is chosen to be defined at the new time step. σ_i^{k+1} then becomes

$$\sigma_i^{k+1} = \frac{\sigma_i^k + E\Delta t_e \frac{u_{i+1}^k - u_i^k}{\Delta x} - \frac{1-k_T}{1+k_T} E\Delta t_e \cdot \Delta_i^k}{1 + \frac{2E\Delta t_e}{(1+k_T)P} \cdot \Delta_i^k} \quad (3.48)$$

Using the definitions of Δ , P and E several additional abbreviations can be made. As they decrease the readability of the expression they are not shown here.

Having updated the ice stresses we step the momentum equation (3.31) forward by Δt_e as follows

$$\rho_i u_i^k \frac{u_i^{k+1} - u_i^k}{\Delta t_e} = \frac{\sigma_i^k - \sigma_{i-1}^k}{\Delta x} + c_a \rho_a u_a |u_a| u_a - c_o \rho_o u_a^k |u_i^k| u_i^k \quad (3.49)$$

or solved for u_i^{k+1}

$$u_i^{k+1} = u_i^k + \frac{\Delta t_e}{\rho_i u_i^k} \left(\frac{\sigma_i^k - \sigma_{i-1}^k}{\Delta x} + c_a \rho_a u_a |u_a| u_a - c_o \rho_o u_a^k |u_i^k| u_i^k \right) \quad (3.50)$$

After solving (3.48) and (3.50) N times, the equivalent ice thickness h and ice concentration a are updated identically to the implementation after the implicit solution of the momentum equation above.

3.5.3 Model setup

The default model specifications are listed in Table 3.2.

This sets up a strip of landfast ice that is attached to a coast (the closed left boundary) that can leave the domain through the open right boundary should

Table 3.2: Default setup of the one-dimensional model.

Size of modeled domain	300 km
Size of grid box	1 km
Advective time step	10 min
Number of elastic time steps per advective time step	250
Initial width of landfast sea ice	100 km
Initial ice thickness of landfast ice	1 m
Initial ice concentration of landfast ice	1
Tensile strength factor k_T	1 ^{a)}
Elasticity constant E_0	0.25
Left boundary condition	closed
Right boundary condition	open
Offshore wind strength	10 m s ⁻¹

a) This means that the tensile strength is set to be equal to the compressive strength of ice ($T = P$).

it break loose.

The tensile strength is set to equal compressive strength. This might be realistic on a micro-scale, i.e. when working with a block of ice, so might be appropriate for a model with a resolution of meters. Floes and landfast ice do reach sizes of several kilometers so it can be expected to see significant effects of tensile strength on the scale of my model. Most models use much larger grid spacing though and thus the effective tensile strength would be expected to be much smaller than the ice's compressive strength. This choice of setting $T = P$ was made here to conceptually illustrate the effect of adding significant tensile strength.

3.6 Results

3.6.1 Analytical solutions

In this section I derive a couple of “back of envelope” results that I will compare to the model output.

Maximum width of landfast ice

Assuming we have a sheet of landfast ice of width L (see Figure 3.5) at rest we can solve the momentum equation (3.31) analytically. The ice velocity is zero

and thus so is the ocean drag. The equation then simplifies to

$$0 = \frac{\partial \sigma}{\partial x} + \tau_a \quad (3.51)$$

respectively

$$\frac{\partial \sigma}{\partial x} = -\tau_a \quad (3.52)$$

i.e. the stress decreases linearly within the ice. With an ice concentration of 1 within the ice, and an idealized offshore (i.e. positive) wind that is constant over time and space the wind stress simplifies to:

$$\tau_a = c_a \rho_a u_a^2 \quad (3.53)$$

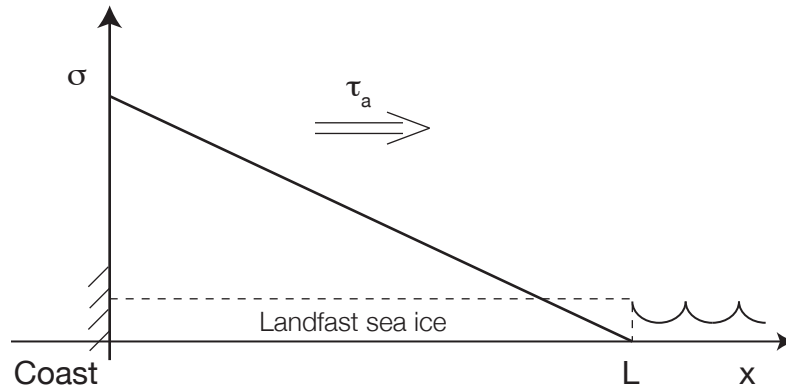


Figure 3.5: Stress (slanted line) in an idealized piece of landfast ice (dashed) under the influence of a constant offshore wind.

The ice stress at the ice edge $\sigma(L)$ is 0, because no ice is pushing against it.

The stress within the ice sheet is then (see Figure 3.5).

$$\sigma(x) = \tau_a(L - x) \quad (3.54)$$

We want to find the maximum width L_{max} of landfast ice that can resist a certain wind stress. The maximum tensile stress that the ice can sustain is T which will be reached at $x = 0$.

$$L_{max} = \frac{\sigma(0)_{max}}{\tau_a} = \frac{T}{\tau_a} = \frac{k_t P}{c_a \rho_a u_a^2} = \frac{k_t P^* h e^{c^*(1-a)}}{c_a \rho_a u_a^2} \quad (3.55)$$

where I assumed again that the equivalent ice thickness is 1 m and the ice concentration is 1.

Further I used parameters as given in Table 3.1 and picked standard values as given in Table 3.2 (in particular an offshore wind of 10 ms^{-1}). We find that landfast ice should be able to sustain itself up to a width of $L_{max} = 212 \text{ km}$.

Creep of ice

The viscous-plastic rheology experiences a slow creep when under a stress between the maximum compressive or tensile stress (see Figure 3.3 and surrounding text). From equation (3.34) we find that the strain rate depends on the stress in the following way:

$$\frac{\partial u}{\partial x} = \left(\sigma(x) - \frac{P - T}{2} \right) \cdot \frac{2 \Delta_{min}}{P + T} = \sigma(x) \cdot \frac{\Delta_{min}}{P} \quad (3.56)$$

where $\sigma(x)$ is the stress profile within the landfast ice (see equation (3.54)). Again choosing our standard values, and in particular $T = P$, the expression simplified considerably ($P - T = 0$ and $P + T = 2P$).

The ice velocity at the coastline is 0, so we can find the velocity at any location x in the landfast ice by integrating $\frac{\partial u}{\partial x}$ away from the coast:

$$\begin{aligned} u(x) &= \int_0^x \frac{\partial u}{\partial x'} dx' = \int_0^x \frac{\Delta_{min}}{P} \sigma(x) dx' = \int_0^x \frac{\Delta_{min}}{P} \tau_a (L - x) dx' \\ &= \frac{\Delta_{min} \tau_a}{P} \left(Lx - \frac{x^2}{2} \right) \end{aligned} \quad (3.57)$$

which is a parabola that goes through the origin and achieves its vertex at the ice edge. The modeled velocity at the ice edge becomes.

$$u(L) = \frac{\Delta_{min} \tau_a}{P} \cdot \frac{L^2}{2} \quad (3.58)$$

Using my typical values the velocity at the ice edge becomes

$$u(100 \text{ km}) = 4.73 \cdot 10^{-5} \text{ ms}^{-1} \quad (3.59)$$

3.6.2 Modeling results

Effect of adding tensile strength

Figure 3.6 shows the effect that adding tensile strength has in the default setup.

The images on the left side show the ice thicknesses h of the regular model without tensile strength, while the right side shows that the ice remains fast after adding tensile strength.

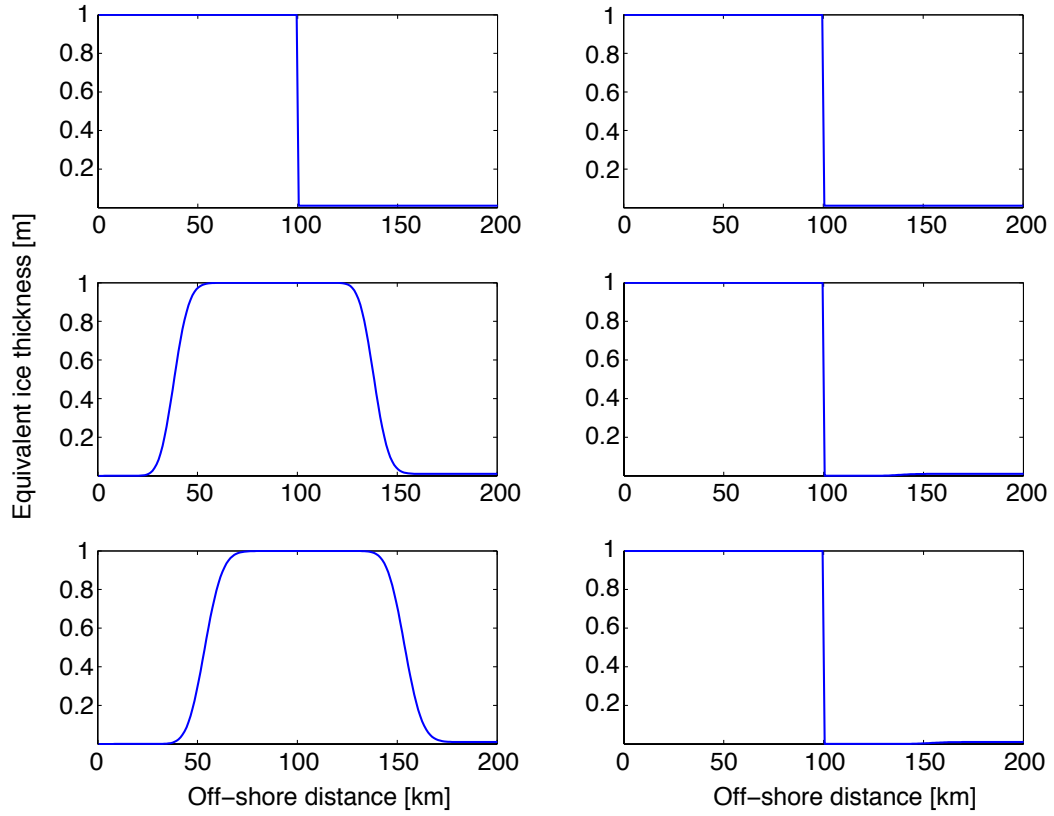


Figure 3.6: Profiles of equivalent ice thickness h as modeled by the implicit implementation of the viscous-plastic rheology. On the left side are the results of the regular model without tensile strength initially, after 2.5 days and after 3.5 days. On the right side are the results after adding tensile strength at the same times.

Comparison of the two rheologies

The implicit method does very well. Figure 3.7 shows the velocity profile within the landfast sea ice after one time step. It approximates the analytical solution from the last section to an accuracy of less than 10^{-6} , which is because the momentum equation was iterated until the solution changed by less than 10^{-6} ms^{-1} .

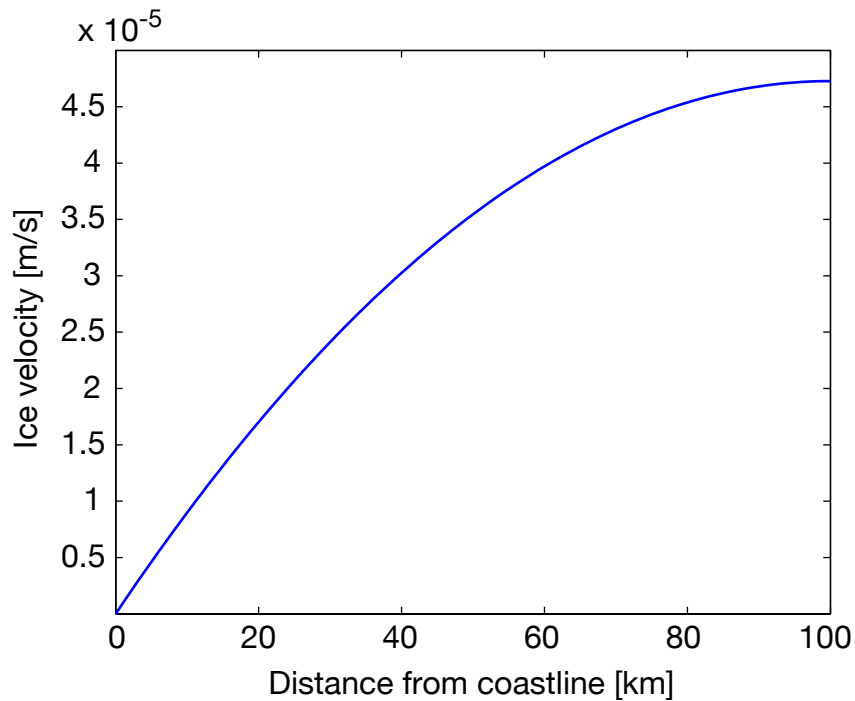


Figure 3.7: Ice velocities within the 100 km of landfast ice after one time step (10 min's) using the implicit solver. In this graph, the analytical solution would be indistinguishable from this curve.

EVP's solution looks quite different, as can be seen in Figure 3.8. Now on

the left side is the solution to the implicit scheme with tensile strength as seen before. On the right side we see the solution of the explicit elastic-viscous-plastic scheme.

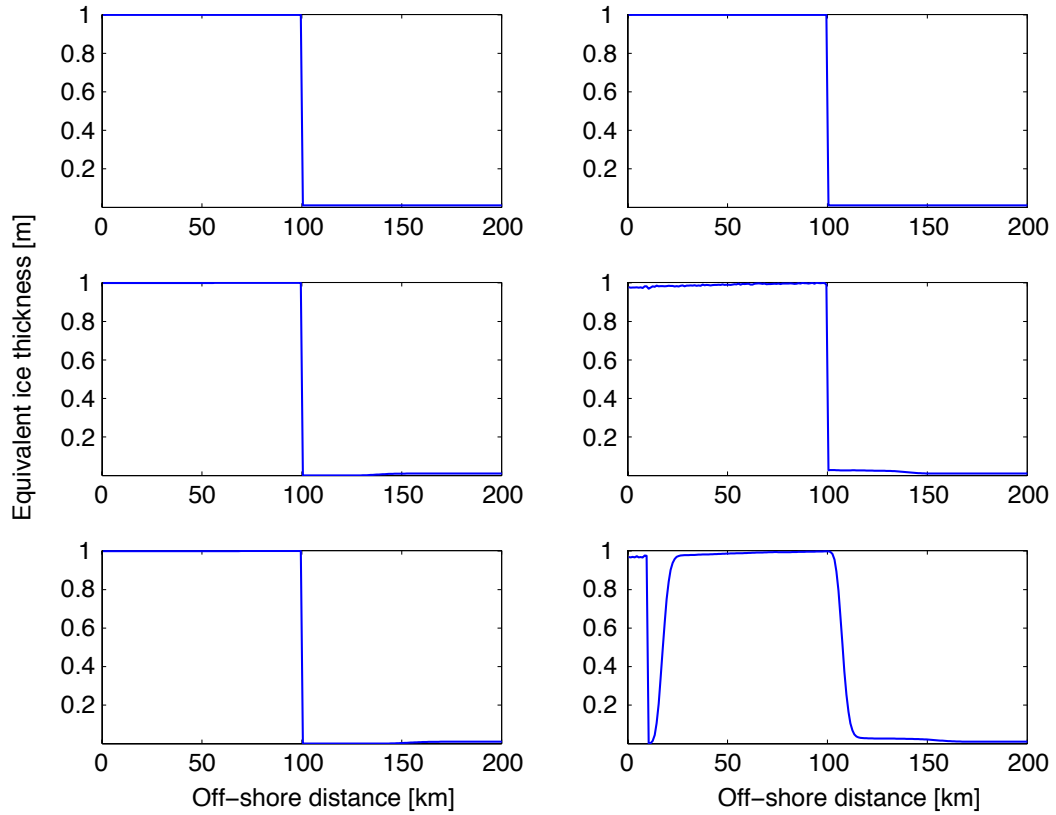


Figure 3.8: Profiles of equivalent ice thickness h . The figures to the left show the solution as found using the implicit scheme, the right side the results using EVP. The top shows the initial condition, the middle two pictures show the state after 2.5 days, the bottom after 3.5 days.

From section 3.6.1 we know that landfast ice up to a width of 212 km should be maintained, so certainly also the 100 km shown here. Indeed that is what

we see on the left side. Using EVP though, the ice breaks off after 3 days.

A closer look at the ice thickness throughout the landfast ice is given in Figure 3.9, where we see on the left side the slow thinning of the ice due to the viscous creep. The thinning on the right side (EVP) is on a much larger scale though (note the difference of scales).

Figure 3.9 also shows how small negative fluctuations can grow more negative. At around 10 km what is a small negative fluctuation after half a day, has grown to a negative spike after 2.5 days and that is where the ice finally breaks off after 3 days.

A closer look at the EVP solution shows large velocity fluctuations during the first few time steps as shown in the top of Figure 3.10. Those fluctuations do die away over time and the velocity profile approaches the shape of the analytical solution except that the velocities are larger by about a factor of 100, on the order of 10^{-3} ms^{-1} . These are still very small velocities and probably insignificant in regular geophysical settings but in this case they change the capability to sustain landfast sea ice drastically.

The initial fluctuations seem to lead to significant initial weakening of the ice sheet (see bottom of Figure 3.10). Once the ice thickness and concentration (not shown) are diminished, the strength of the ice sheet is significantly reduced, which leads to faster creep rates, which again leads to an accelerated thinning of the ice. This leads to landfast ice breaking off much earlier than expected.

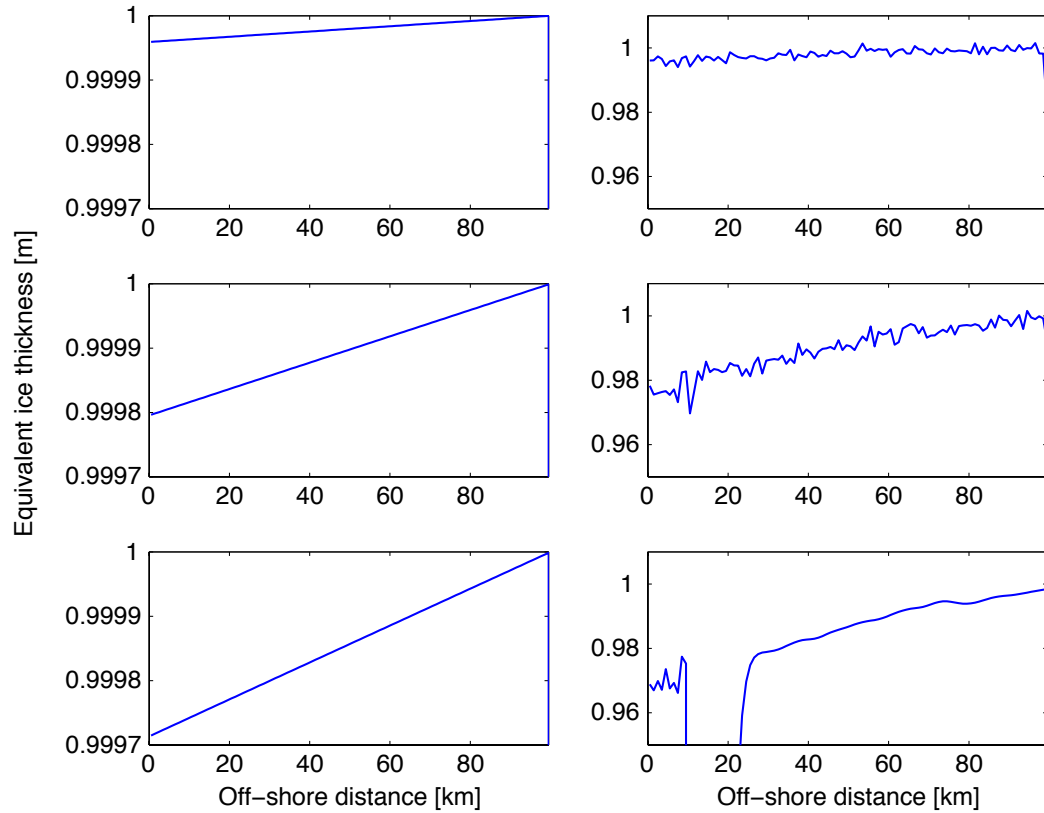


Figure 3.9: The top two figures show the equivalent ice thickness after 0.5, 2.5 and 3.5 days (top to bottom). The figures to the left show the solution as found using the implicit scheme, the right side the results using EVP. Only the first 100 km are shown (ice extent). Note that the scales differ between the left and the right column.

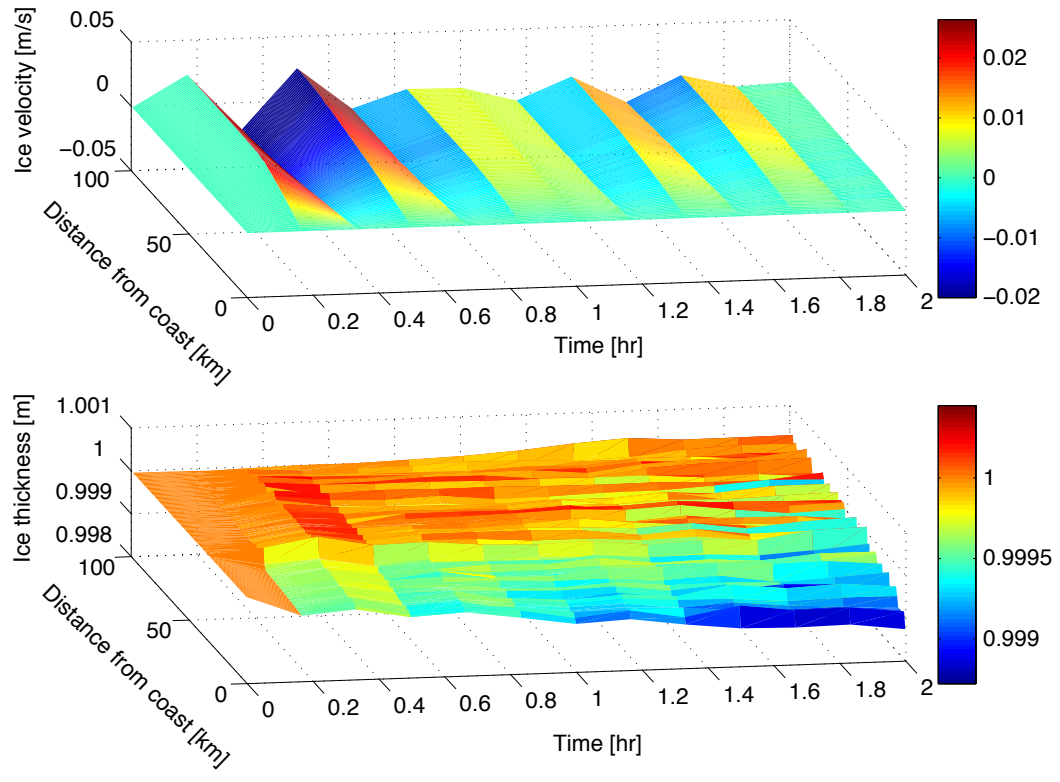


Figure 3.10: Initial velocity fluctuations (on top) and the development of the ice thickness during the same time (on the bottom).

The question arises what causes these fluctuations. Is this a result of the elastic term or a numerical problem?

Figure 3.11 shows a comparison of the initial fluctuations with the same model using a time step that is a ten times smaller (1 min instead of 10 min). The fluctuations look stunningly similar except that the velocities as well as the time scale are also tenth as large. And indeed, running the model with the smaller time step, break off happens after over 40 days (as compared to around 3 days with the regular time step). due to the reduced velocity fluctuations and accompanying weakening of the ice.

It seems thus that EVP indeed converges to the viscous-plastic rheology when choosing small time steps but that initial elastic effects have a detrimental influence on the stability of the landfast ice.

Either way, the ice managed to remain fast for a significant time under strong offshore winds. The question becomes for how long landfast ice of a certain width may remain fast.

Figure 3.12 shows the widths of initial landfast sea ice that remained fast for a certain number of days (to an accuracy of six hours and up to a maximum of 40 days).

Again one sees that the implicit solution approaches the theoretical expectations. As we did not consider the effect of creep in the calculations, it had to be expected that the ice would break off after some time. EVP on the other

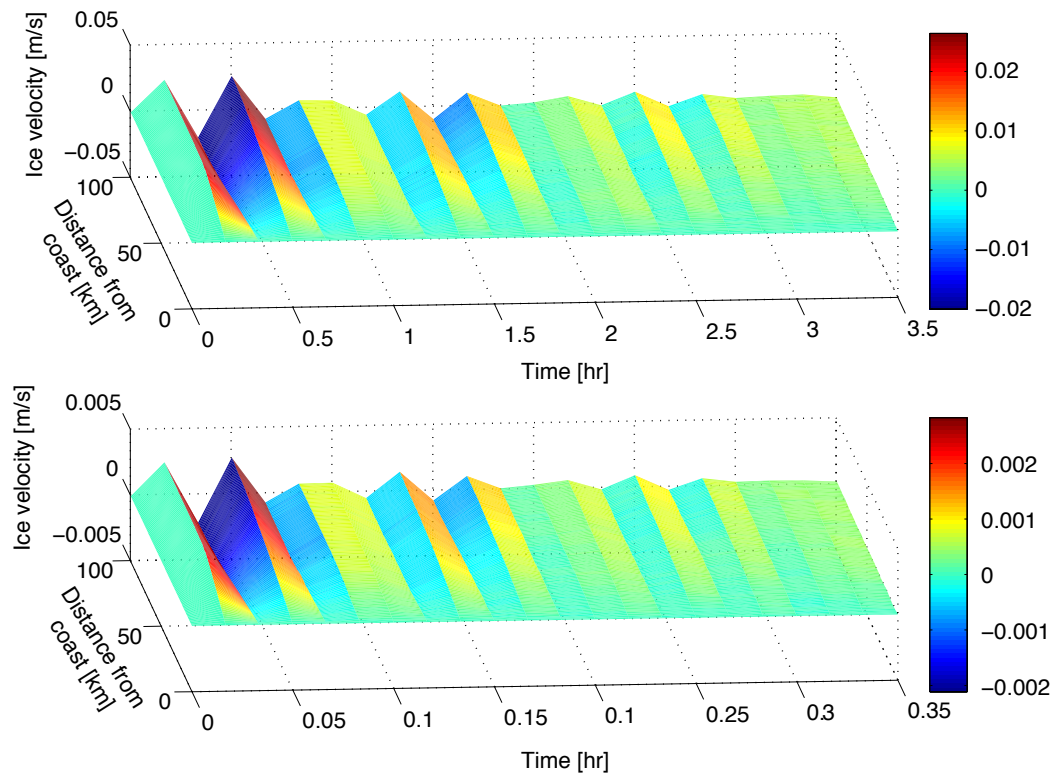


Figure 3.11: Initial velocity fluctuations in the EVP model. The top figure shows velocities when using a time step of 10 minutes, while the bottom figure uses a time step of 1 minute. Note the different scales in time as well as velocities.

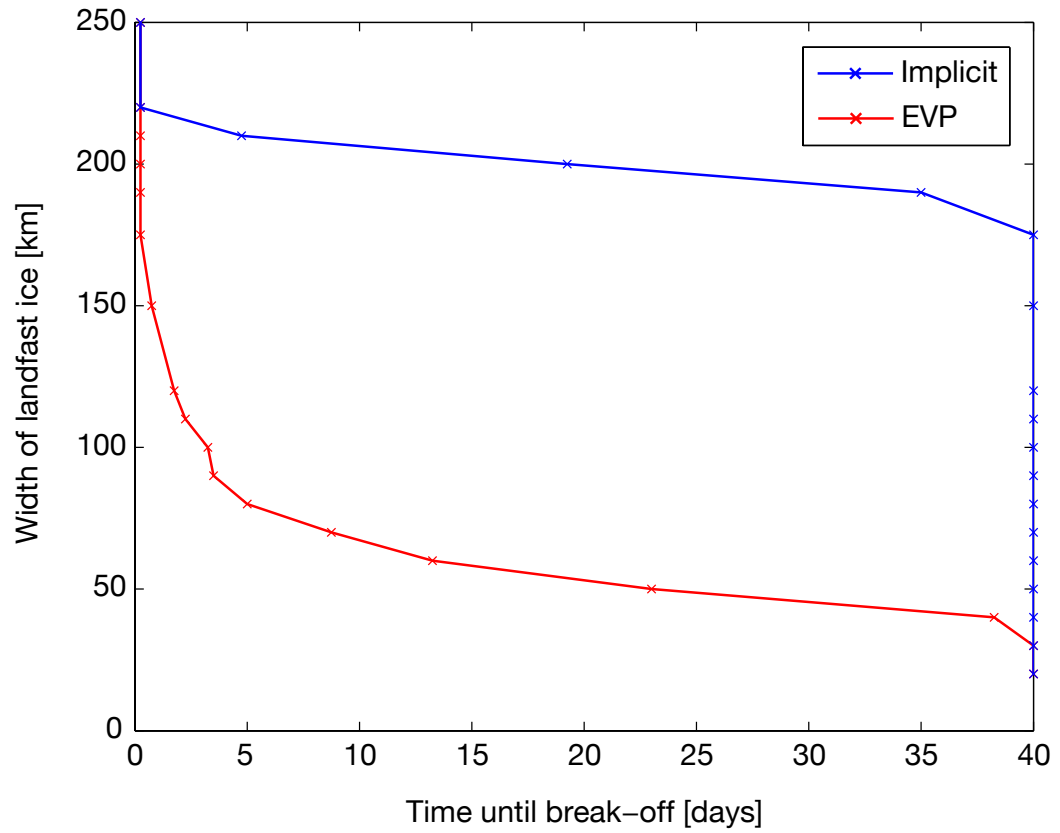


Figure 3.12: Number of days until landfast ice of a certain width breaks off under the influence of offshore wind.

hand manages to sustain only about a third of the expected width of landfast ice over a significant time duration.

3.7 Discussion

The implicit solution to VP does almost as good as our theoretical solution predicted. 210 km of landfast ice break off within 5 days but as our calculations did not consider the slow creep that weakens the ice, this is not astonishing.

EVP has the tendency of breaking off much faster. I suggest that this is due to initial elastic waves that weaken the ice. Still widths of over 50 km remain fast for several weeks, which can be considered realistic.

In all cases the ice always breaks at or very close to the coastline. This is expected from our model as the ice stress is largest there and it is there where the atmospheric pull would exceed the tensile strength of the ice. In reality, breaking can take place anywhere and often is observed farther away from the coast (Wadhams, 1986). It is likely that other effects like for example action of waves or tides, collisions with pack ice or thermodynamics play a role.

Ultimately, to decide if adding tensile strength to an ice rheology improves the modeling of landfast sea ice, one has to run the modified model including ice thermodynamics on a realistic domain with realistic atmospheric and oceanic forcing (from data or models) and compare the outcome with high resolution

sea ice data. This will also allow to find appropriate values for T respectively k_T .

Another open question is the effect of added tensile strength to the ice flow in the ice pack. Again only more realistic modeling studies will be able to identify positive or negative effects. Presumably adding significant tensile strength to the ice pack would not improve modeling there and a combined model might be appropriate; one that treats ice differently in the pack or close to land. Some measurements have indicated that some physical parameters differ fundamentally between pack and fast ice (Prinsenberg et al., 1997) so that such a “phase change” might be needed to properly model landfast sea ice.

Bibliography

D. J. Acheson. *Elementary Fluid Dynamics*. Oxford Applied Mathematics and Computing Science Series. Oxford University Press, 1990.

Arctic Climate Impact Assessment Modeling and Scenarios Workshop, Stockholm, Sweden, January 19-21 2001. ACIA.

D. G. Barber and J. M. Hanesiak. Meteorological forcing of sea ice concentrations in the southern Beaufort Sea over the period 1979 to 2000. *Journal of Geophysical Research*, 109(C06014), 2004.

I. Bratchie. Rheology of an ice-floe field. *Annals of Glaciology*, 5:23–28, 1984.

K. Bryan, S. Manabe, and R. L. Pacanowski. A global ocean-atmosphere climate model. Part II: The oceanic circulation. *Journal of Physical Oceanography*, 5:30–46, 1975.

W. J. Campbell. The wind-driven circulation of ice and water in a polar ocean. *Journal of Geophysical Research*, 70:3279–3301, 1965.

MANICE - Manual of Standard Procedures for Observing and Reporting Ice Conditions. Canadian Ice Service - Environment Canada, 373 Sussex Drive, LaSalle Academy, Block 'E', Ottawa, Ontario K1A 0H3, ninth edition, April 2002.

R. Colony and R. S. Pritchard. Integration of elastic-plastic constitutive laws. *AIDJEX Bulletin*, 30:55–80, 1975.

M. D. Coon. A review of AIDJEX modeling. In R. S. Pritchard, editor, *Sea ice processes and models*, pages 12–25. University of Washington Press, 1980.

M. D. Coon, G. A. Maykut, R. S. Pritchard, and D. A. Rothrock. Modeling pack ice as an elastic-plastic material. *AIDJEX Bulletin*, 24:1–105, May 1974.

D. V. Divine, R. Korsnes, A. P. Makshtas, F. Godtliobsen, and H. Svendsen. Atmospheric-driven state transfer of shore-fast ice in the northeastern Kara Sea. *Journal of Geophysical Research*, 110(C09013), 2005.

J. A. Dumas, G. M. Flato, and R. D. Brown. Future projections of landfast ice thickness and duration in the Canadian Arctic. *Journal of Climate*, 19: 5175–5189, Oct 2006.

D. R. Durran. *Numerical methods for wave equations in geophysical fluid dynamics*, volume 32 of *Texts in Applied Mathematics*. Springer-Verlag New York, 1999.

- A. I. Felzenbaum. The theory of steady drift of ice and the calculation of the long period mean drift in the central part of the Arctic Basin. *Problems of the North*, 2:13–44, 1961.
- F. Fetterer and V. Troisi. AARI 10-day Arctic ocean EASE-grid sea ice observations. Boulder, CO, USA: National Snow and Ice Data Center. Digital media, 1997a.
- F. Fetterer and V. Troisi. Data set documentation to AARI 10-day Arctic ocean EASE-grid sea ice observations, 1997b. URL http://nsidc.org/data/docs/daac/nsidc0050_aari_ease_seaice.gd.html.
- G. M. Flato and W. D. Hibler. Modeling pack ice as a cavitating fluid. *Journal of Physical Oceanography*, 22:626–651, June 1992.
- J. N. Goodier and P. G. Hodge. *Elasticity and Plasticity*. Wiley, 1958.
- J. M. N. T. Gray and Peter D. Killworth. Stability of the viscous-plastic sea ice rheology. *Journal of Physical Oceanography*, 25:971–978, May 1995.
- J. M. N. T. Gray and L. W. Morland. A two-dimensional model for the dynamics of sea ice. *Philosophical Transactions: Physical Sciences and Engineering*, 347 (1682):219–290, 1994.
- W. D. Hibler. A viscous sea ice law as a stochastic average of plasticity. *J. Geophys. Res.*, 82(27):3932–3938, 1977.

- W. D. Hibler. A dynamic thermodynamic sea ice model. *Journal of Physical Oceanography*, 9:815–846, July 1979.
- W. D. Hibler. Modeling a variable thickness sea ice cover. *Monthly Weather Review*, 108:1943–1973, December 1980.
- W. D. Hibler. Ice dynamics. In Norbert Untersteiner, editor, *The Geophysics of Sea Ice*, volume 146 of *NATO ASI, Series B, Physics*, pages 577– 640. Plenum Press, New York, 1986.
- W. D. Hibler and E. Schulson. On modeling anisotropic failure and flow of flawed sea ice. *Journal of Geophysical Research*, 105:17105 – 17120, 2000.
- D. M. Holland. A 1-d elastic-plastic sea-ice model solved with an implicit Eulerian-Lagrangian method. *Ocean Modelling*, (accepted), 2006.
- E. C. Hunke and J. K. Dukowicz. An elastic-viscous-plastic model for sea ice dynamics. *Journal of Physical Oceanography*, 27:1849–1867, September 1997.
- C. F. Ip, W. D. Hibler, and G. M. Flato. On the effect of rheology on seasonal sea-ice simulations. *Annals of Glaciology*, 15:17–25, 1991.
- O. M. Johannessen, M. Miles, and E. Bjørgo. The Arctic’s shrinking sea ice. *Nature*, 376:126–127, July 1995.

- E. Kalnay et al. The NCEP/NCAR 40-year reanalysis project. *Bulletin of the American Meteorological Society*, 77(3):437–470, 1996.
- J. L. Lieser. *A numerical model for short-term sea ice forecasting in the Arctic*. PhD thesis, Universität Bremen, 2004.
- R. W. Macdonald, D. W. Paton, E. C. Carmack, and A. Omstedt. The freshwater budget and under-ice spreading of Mackenzie river water in the Canadian Beaufort Sea based on salinity and $^{18}\text{O}/^{16}\text{O}$ measurements in water and ice. *Journal of Geophysical Research*, 100(C1):895–919, 1995.
- R. W. Macdonald, E. C. Carmack, and D. W. Paton. Using the $\delta^{18}\text{O}$ composition in landfast ice as a record of Arctic estuarine processes. *Marine Chemistry*, 65:3–24, 1999.
- S. Manabe, K. Bryan, and M. J. Spelman. A global ocean-atmosphere climate model with seasonal variation for future studies of climate sensitivity. *Dynamics of Atmospheres and Oceans*, 3:393–426, 1979.
- M. G. McPhee. Ice-ocean momentum transfer for the AIDJEX ice model. *AIDJEX Bulletin*, 29:93–111, 1975.
- J. M. Oberhuber. Simulation of the Atlantic circulation with a coupled sea ice-mixed layer-isopycnal general circulation model. Part I: Model description. *Journal of Physical Oceanography*, 23(5):808–829, May 1993.

- C. L. Parkinson and W. M. Washington. A large-scale numerical model of sea ice. *Journal of Geophysical Research*, 84:311–337, 1979.
- E. P. Popov. *Mechanics of materials*. Prentice-Hall., 1952.
- S. J. Prinsenbergh, A. Van der Baaren, G. A. Fowler, and I. K. Peterson. Pack ice stress and convergence measurements by satellite-tracked ice beacons. In *OCEANS '97. MTS/IEEE Conference Proceedings*, volume 2, pages 1283–1289, 6-9 Oct 1997.
- R. S. Pritchard. Long-term sea ice dynamics simulations using an elastic-plastic constitutive law. *Journal of Geophysical Research*, 106(C12):31333–31344, 2001.
- R. S. Pritchard. An elastic-plastic constitutive law for sea ice. *Journal of Applied Mechanics*, 42E:379–384, 1975.
- D. A. Rothrock. The mechanical behavior of pack ice. *Annual Review of Earth and Planetary Sciences*, 3:317 – 342, 1975.
- D. A. Rothrock, Y. Yu, and G. A. Maykut. Thinning of the Arctic sea-ice cover. *Geophysical Research Letters*, 26(23):3469–3472, December 1999.
- S. Rysgaard, T. G. Nielsen, and B. W. Hansen. Seasonal variation in nutrients, pelagic primary production and grazing in a high-Arctic coastal marine

- ecosystem, Young Sound, Northeast Greenland. *Marine Ecology Progress Series*, 179:13–25, April 1999.
- R. M. S. M. Schulkes. Asymptotic stability of the viscous–plastic sea ice rheology. *Journal of Physical Oceanography*, 26(2):279–283, February 1996.
- D. T. Shindell, R. L. Miller, G. A. Schmidt, and L. Pandolfo. Simulation of recent northern winter climate trends by greenhouse-gas forcing. *Nature*, 399:452–455, June 1999.
- R. J. Stouffer, S. Manabe, and K. Bryan. Interhemispheric asymmetry in climate response to a gradual increase of atmospheric CO₂. *Nature*, 342:660–662, December 1989.
- L.-B. Tremblay and L. A. Mysak. Modeling sea ice as a granular material, including the dilatancy effect. *Journal of Physical Oceanography*, 27:2342–2360, 1997.
- L.-B. Tremblay and L. A. Mysak. The possible effects of including ridge-related surface roughness in air-ice drag parameterization: a sensitivity study. *Annals of Glaciology*, 25:22–25, 1998.
- C. T. Tynan and D. P. DeMaster. Observations and predictions of Arctic climatic change: Potential effects on marine mammals. *Arctic*, 50(4):308–322, 1997.

- V. A. Volkov, O. M. Johannessen, V. E. Borodachev, G. N. Voinov, L. H. Pettersson, L. P. Bobylev, and A. V. Kouraev. *Polar Seas Oceanography: An integrated case study of the Kara Sea*. Springer-Verlag New York, 2002.
- P. Wadhams. The seasonal ice zone. In Norbert Untersteiner, editor, *The Geophysics of Sea Ice*, volume 146 of *NATO ASI, Series B, Physics*, pages 826–835. Plenum Press, New York, 1986.
- J. Zhang and D. A. Rothrock. Effect of sea ice rheology in numerical investigations of climate. *Journal of Geophysical Research*, 110(C08014), 2005.
- D. Zyryanov, D. V. Divine, and R. Korsnes. Mechanical simulation of shore fast ice breakup: Kara and Laptev seas. Paper presented at the International Workshop on Small-Scale Sea Ice-Ocean Modeling for Nearshore Beaufort and Chukshi Seas, Int. Arctic Res. Cent., Fairbanks, Alaska, 8-9 Aug 2002.